

Open star clusters and their asymmetrical tidal tails

PAVEL KROUPA,^{1,2} JAN PFLAMM-ALTENBURG,¹ SERGIJ MAZURENKO,³ WENJIE WU,¹ INGO THIES,¹ VIKRANT JADHAV,¹ AND
TEREZA JERABKOVA⁴

¹*Helmholtz-Institut für Strahlen- und Kernphysik
Universität Bonn, Nussallee 14-16*

53115 Bonn, Germany

²*Astronomical Institute*

Charles University, V Holesovickach 2

18000 Praha, Czech Republic

³*Universität Bonn*

Regina-Pacis-Weg 3

53113 Bonn, Germany

⁴*European Southern Observatory*

Karl-Schwarzschild-Strasse 2

85748 Garching, Germany

ABSTRACT

Stars that evaporate from their star cluster by the energy equipartition process end up either in a leading or a trailing tidal tail. In Newtonian gravitation and for open star clusters in the Solar vicinity, the tidal threshold, or práh, for escape is symmetrical, such that the leading and trailing tails are equally populated. The data by six independent teams that applied the convergent point method to map out the tidal tails of four open clusters (the Hyades, the Praesepe, Coma Berenices and COIN-Gaia13) using Gaia DR2 and DR3 are here applied to test for the expected symmetry. All tidal tails contain more stars in the leading tail. The combined confidence amounts to an 8σ falsification of the práh symmetry. The same test using Milgromian dynamics leads to consistency with the data. More effort needs to be exerted on this matter, but the data indicate with high confidence that the tidal práh of an open star cluster is asymmetrical with the corresponding confidence that Newtonian gravitation is falsified. Open star clusters depopulate more rapidly in Milgromian than in Newtonian dynamics and the COIN-Gaia13 cluster is here found to be nearly completely dissolved. In view of these results, the wide-binary star test and the Keplerian Galactic rotation curve finding are briefly discussed.

Keywords: Open star clusters(1160) — Star clusters(1567) — Tidal tails(1701) — Gravitation(661)
— Newtonian gravitation(1110) — Modified Newtonian dynamics(1069)

1. INTRODUCTION

The stars in an open cluster with initial mass $M_{oc,0}$ orbit chaotically within it with the many weak gravitational encounters leading to an on-going redistribution of kinetic energy amongst them as the cluster evolves towards energy equipartition which cannot be reached. As a consequence of this two-body-relaxational process there is a near-constant rate of loss of stars across the

tidal threshold, or práh¹, $\dot{M}_{oc} \propto M_{oc,0}$ (eq. 12 in Baumgardt & Makino 2003). By virtue of the stars leaking out of their cluster having nearly the same velocity as the cluster, they are on very similar Galactocentric orbits thus either drifting ahead or behind the cluster. Capuzzo Dolcetta et al. (2005), followed by Montuori et al. (2007, 2008), were the first to show how the observed tails of some star clusters in the Galaxy take their

Corresponding author: Pavel Kroupa
pkroupa@uni-bonn.de

¹ We adopt this term for the tidal threshold in connection with Milgromian dynamics following Kroupa et al. (2022) where an explanation of its meaning related to the foundation of Prague “on the threshold to a mystical world” is provided.

shape and how and why the (observed) under- and over-densities are theoretically found and explained. Their work was later confirmed and, also, interpreted in terms of epicyclic orbits (Küpper et al. 2008; Just et al. 2009). Tidal tails grow constantly and uniformly in length for open star clusters on almost circular Galactocentric orbits (fig. 7 in Küpper et al. 2010). Owing to the linearity of Newtonian gravitation and near the Solar circle and at larger Galactocentric distances, for such star clusters the leading and trailing tails contain, within Poissonian fluctuations, the same number of stars. The symmetry of the tail populations has been quantified by Pflamm-Altenburg et al. (2023), who show the evaporation process to be stochastic and describable as a Bernoulli process. This allows quantifying the number of stars in the leading, n_l , and in the trailing tail, n_t , and also how likely a certain degree of asymmetry is, given a total number of detected tail stars, $n = n_l + n_t$.

The notion to test whether Newtonian gravitation is valid on the scales of open star clusters by using n_l and n_t was introduced in Kroupa et al. (2022) based on the new compact convergent point (CCP) method developed by Jerabkova et al. (2021) to map out the full extent of cluster tidal tails. These latter authors quantified for the first time the full length of the tidal tails of the Hyades, Praesepe and Coma Berenice, and later also of NGC 752 (Boffin et al. 2022). By applying Milgromian and Newtonian gravitational models to these data, Kroupa et al. (2022) showed that while the full tails of the Praesepe, Coma Berenices and NGC 752 are consistent with Newtonian symmetry, the data are also consistent with Milgromian gravitation. The full-length tails of the Hyades cluster, however, are inconsistent with the Newtonian symmetry at more than 5σ confidence (see also Pflamm-Altenburg et al. 2023), while being consistent with Milgromian gravitation. The Galactic bar does not influence the evolution of star clusters orbiting at Galactocentric distances larger than ≈ 4 kpc (Rossi & Hurley 2015). Thomas et al. (2023) subsequently showed that the Milky Way’s non-axisymmetric bar potential cannot lead to the observed asymmetry. The significant Hyades tail asymmetry thus supports the possibility that the *práh* is Milgrom-asymmetric, namely, that more stars escape per unit time on the Galaxy-near side of the open cluster than on the far side.

If this were to be affirmed with additional data then we would be forced to discard Newtonian gravitation with corresponding implications for all of galactic, extragalactic and cosmological research. The tidal tail data clearly need significant improvement to either confirm or discard the Milgrom-asymmetric *práh*. The aim here is to test data on tidal tails of open star clusters

that have been obtained with the established convergent point (CP) method and by research teams operating independently of the Jerabkova et al. and Kroupa et al. efforts and prior to the publication of Kroupa et al. (2022). These latter authors made the observation (their sec. 2.2) that the tidal-tail-data extracted for the Hyades, Praesepe, COIN-Gaia13 and Coma Berenices by six different teams using the standard CP method appear to show an asymmetry by the leading tail having more stars than the trailing tail. This asymmetry based on data extracted using the CP method was not quantified though, and instead the new tidal tail data extracted using the new CCP method were used. Here we return to the previous CP-based observations that were obtained prior to the invention of the CCP method. Thus, while in Kroupa et al. (2022) extended tidal tail data in the distance range 50 to 200 pc ahead and behind the three clusters Hyades, Praesepe and Coma Berenices and in the distance range 50 to 130 pc ahead and behind the cluster NGC 752 were used, here we restrict the distance range from 10 pc to an upper distance value for which data is reported by the six different teams that used the CP method. The CP method is well known and finds candidate ex-cluster members that co-move with the cluster and that are still in the vicinity of the cluster (typically to within about 150 pc). The more involved new CCP method instead can identify more distant candidate ex-cluster-members. But it relies on a model of the tidal tail because the CP method breaks down when the linearity assumption is violated since the stars increasingly deviate from the cluster centre-of-mass velocity: as they drift further from the cluster they are accelerated in the Galactic potential. Here we ignore the cluster NGC 752 used in Kroupa et al. (2022) because this cluster does not have tidal tail information that was published prior to the invention of the CCP method. The Milgromian models reported in Kroupa et al. (2022) were consistent with the tidal tail data of the three clusters Hyades, Praesepe and Coma Berenices, but the extended tidal tail data of the Hyades were asymmetric with more than 5σ confidence. The tidal tails of the two other clusters did not indicate a strong asymmetry. Here we use the same three clusters but rely on the less-extended tidal tail data extracted prior to the invention of the CCP method using the more robust CP method and we add the cluster COIN-Gaia13 for which such data also exist. These data on the tidal tails closer to the open clusters are more sensitive to the potential of the cluster plus Galaxy combination since they assess the more recent escape of stars through the *práh*.

The here-used data and the analysis as to their possible tidal práh asymmetry are introduced in Sec. 2 and in Sec. 3, respectively. The Milgromian and Newtonian models are compared with these data in Sec. 4 and the results are presented in Sec. 5. Sec. 6 contains the conclusions with a brief discussion of recent advances concerning the validity of Milgromian and Newtonian dynamics.

2. THE CLUSTER DATA

The astrometric quality of the Gaia data release 2 (DR2) allows stars to be extracted from the surroundings of four nearby open clusters that most likely originated from the respective clusters. The standard CP method (see Jerabkova et al. 2021 and references therein) was applied by six different teams on the Hyades (Röser et al. 2019; Meingast & Alves 2019), the Praesepe (Röser & Schilbach 2019), COIN-Gaia13 (Bai et al. 2022, using Gaia EDR3) and Coma-Berenices (Fürnkranz et al. 2019; Tang et al. 2019) open clusters. This method picks-up likely cluster ex-members based on their very similar space motion as that of the cluster, and can therefore only map out the ex-members in the vicinity of the cluster to a maximal distance d_{\max} beyond which the CP approach breaks down. With the new CCP method, Jerabkova et al. (2021) introduce a phase-space transformation allowing also the ex-members in the full-length tidal tails to be found. As reasoned in Sec. 1, here we resort only to the previous work based on the CP method, as we aim to be as conservative as possible in testing gravitational theory on the cluster práh.

The position and velocity data of the clusters are from the respective publications, as collated in Table 1. The Galactocentric Cartesian coordinate system X, Y, Z has X including the Galactic Centre and pointing from the anchor-point towards the Galactic centre, the explicit definition depending on various authors' usage with the X -anchor-point sometimes being the Sun, the position of the cluster or local standard of rest (see also Sec. 4). Galactic rotation is in the positive Y direction and the Galactic North pole in the positive Z direction.

The cluster COIN-Gaia13 needs special attention: The data are obtained from Bai et al. (2022) who provide a total number of stars of 478 and a total mass of $439 M_{\odot}$. Based on the local Oort constants they calculated a tidal radius of 11 pc. However, the stellar sample is spread up to a distance of 200 pc from the cluster centre. The majority of the stellar mass used for the calculation of the tidal radius lies outside of the cen-

tral 11 pc radius. In order to derive the proper star cluster (tidal) mass and the corresponding half mass radius we extract² the data from fig. 9 (left) in Bai et al. (2022) which shows the relative cumulative mass fraction of the stellar sample with a mass less than and above $1 M_{\odot}$. Fig. 1 shows the relative cumulative radial mass distribution, with r being the three-dimensional distance from the cluster centre, which is here interpolated by

$$\frac{M(\leq r)}{M_{i,\text{tot}}} = \begin{cases} \rho_1 r & ; \quad r < r_1, \\ \rho_1 r_1 + \rho_2(r - r_1) & ; \quad r_1 \leq r < r_2, \\ \rho_1 r_1 + \rho_2(r_2 - r_1) + \\ (1 - \rho_1 r_1 + \rho_2(r_2 - r_1)) \times \\ (1 - e^{-\rho_3(r - r_2)}) & ; \quad r_2 \leq r, \end{cases} \quad (1)$$

with parameters $r_1 = 45$ pc, $\rho_1 = 0.012$ pc⁻¹, $r_2 = 120$ pc, $\rho_2 = 0.0043$ pc⁻¹ and $\rho_3 = 0.035$ pc⁻¹, and $M_{i,\text{tot}}$ being the total mass of the n stars.

The required internal tidal mass, M_t , of a star cluster as a function of the tidal radius, r_t , in a disk galaxy with differential rotation is given by (Pinfield et al. 1998)

$$M_t(r_t) = \frac{2(A - B)^2}{G} r_t^3, \quad (2)$$

where A and B are the local Oort's constants. Here we use $A = 14.5$ km s⁻¹ kpc⁻¹ and $B = -13.0$ km s⁻¹ kpc⁻¹ from Piskunov et al. (2006). The intersection of this radial tidal mass function, Eq. 2, and the radial cumulative mass distribution (Fig. 1) determines a tidal mass of $M_t = M_{\text{oc}} = 29 M_{\odot}$ and the tidal radius to be $r_t \approx 5.6$ pc (Fig. 2, see e.g. Röser et al. 2011 for the method). It follows that COIN-Gaia13 has a half mass radius of $r_h \approx 4.4$ pc and a Plummer parameter $b \approx 3.4$ pc. These values supersede those reported by Bai et al. (2022).

Because the open clusters are on near-circular orbits about the Galactic centre with relatively small excursions above and below the mid-plane, we analyse the star-counts by projecting the data onto the $X - Y$ plane, as shown in Fig. 3. For each of the six measurements, a line passing through the cluster centre but at right angle to the respective cluster's velocity vector in the $X - Y$ plane is constructed and stars that are 10 pc ahead and behind this line in the $X - Y$ plane are counted as being in the leading and trailing tails, respectively. We use a nominal distance of 10 pc ahead and behind the cluster because this is observationally pragmatic and is similar to the tidal radius, $r_{\text{tid}} \approx (0.5 M_{\text{oc}}/M_{\text{gal}})^{1/3} D_{\odot} \approx 11$ pc

² WEBPLOTDIGITIZER at <https://automeris.io>

Table 1. Data of the present-day star clusters and tidal tails

Cluster	T	\bar{T}	b	X, Y, Z	V_X, V_Y, V_Z	n_l	n_t	d_{\max}
	(Myr)	(Myr)	(pc)	(pc)	(pc/Myr)			(pc)
(1)	(2)	(3)	(4)	(5)	(6)	(7)	(8)	(9)
Hyades(Röser et al. 2019)	580–720	650	3.1	−8344.44, 0.06, 10.22	−32.01, 212.37, 6.13	234	184	175
Hyades(Meingast & Alves 2019)	“	“	“	“	“	40	38	120
Praesepe(Röser & Schilbach 2019)	708–832	770	3.7	−8441.57, −68.90, 127.03	−32.56, 216.53, −2.74	214	124	210
COIN-Gaia13(Bai et al. 2022)	150–350	250	3.4	−8621.0, 109.3, 65.3	28.86, 243.83, −3.82	222	77	210
Coma Ber(Fürnkranz et al. 2019)	700–800	750	2.7	−8306.71, −5.91, 112.44	9.12, 236.90, 6.43	44	21	35
Coma Ber(Tang et al. 2019)	“	“	“	“	“	8	5	35

NOTE—Except for Gaia-COIN13, the ages (T) and Galactocentric position and velocities stem from table 1 in Kroupa et al. (2022). \bar{T} is the mean of the given ages. The Plummer parameters b are from Pflamm-Altenburg et al. (2023) for the Hyades, Praesepe and Coma Berenices. The derivation of the Plummer parameter of COIN-Gaia-13 is described in Sect. 2 (the corresponding half-mass radii being $r_h \approx 1.305b$, e.g. Kroupa 2008). The number of reported candidate stars in the leading and trailing tail of each cluster, n_l, n_t , respectively (see Fig. 3), stem from the respective authors applying the standard CP method. The maximum extent of the tidal tail as obtained by these authors is d_{\max} .

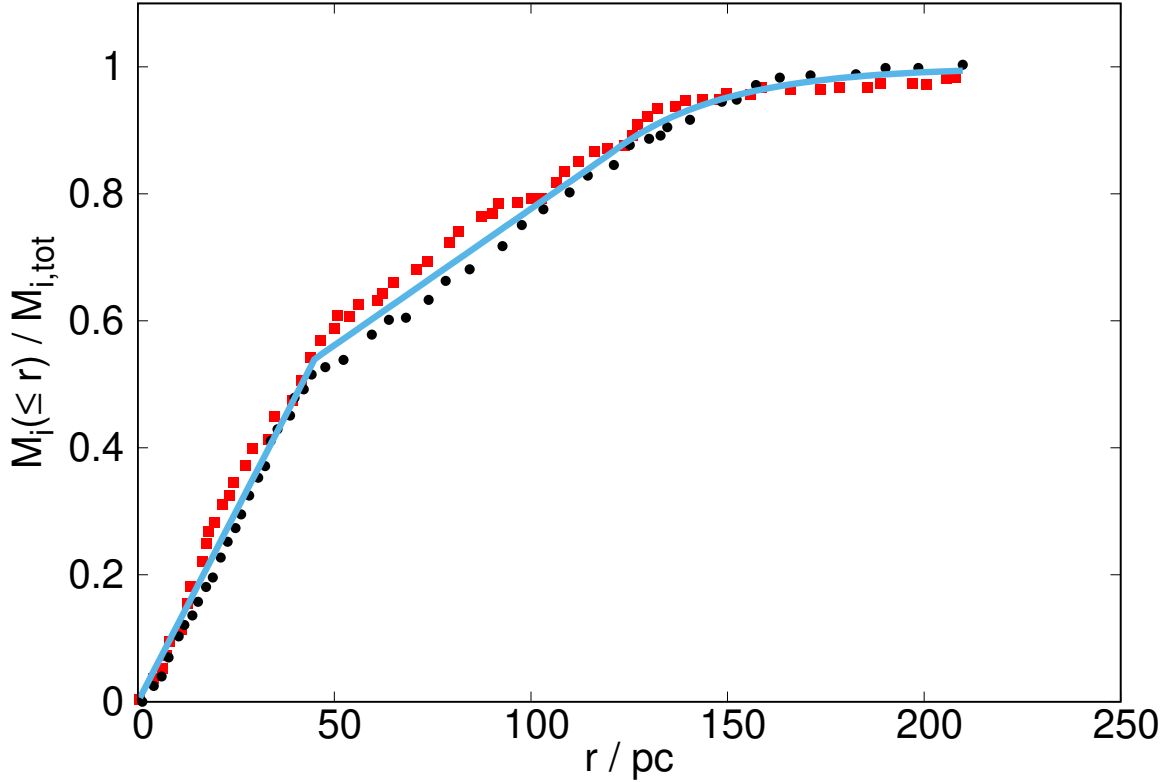


Figure 1. COIN-Gaia13: Radial relative cumulative mass distribution, $M_i(\leq r)$, of stars with masses $m_i < 1 M_\odot$ (squares) and $m_i \geq 1 M_\odot$ (circles). The total mass in all i stars is $M_{i,\text{tot}}$. The solid line shows the interpolation function in Eq. 1.

for an open cluster weighing $M_{\text{oc}} = 300 M_\odot$ at the distance of $D_\odot = 8300 \text{ pc}$ from the Galactic centre in a logarithmic potential corresponding to a Galactic mass

of $M_{\text{gal}} = 0.6 \times 10^{11} M_\odot$ within D_\odot . The masses of the clusters in Table 1 are (table 1 in Kroupa et al. 2022) $M_{\text{oc}} = 275 M_\odot$ (Hyades), $311 M_\odot$ (Praesepe) and

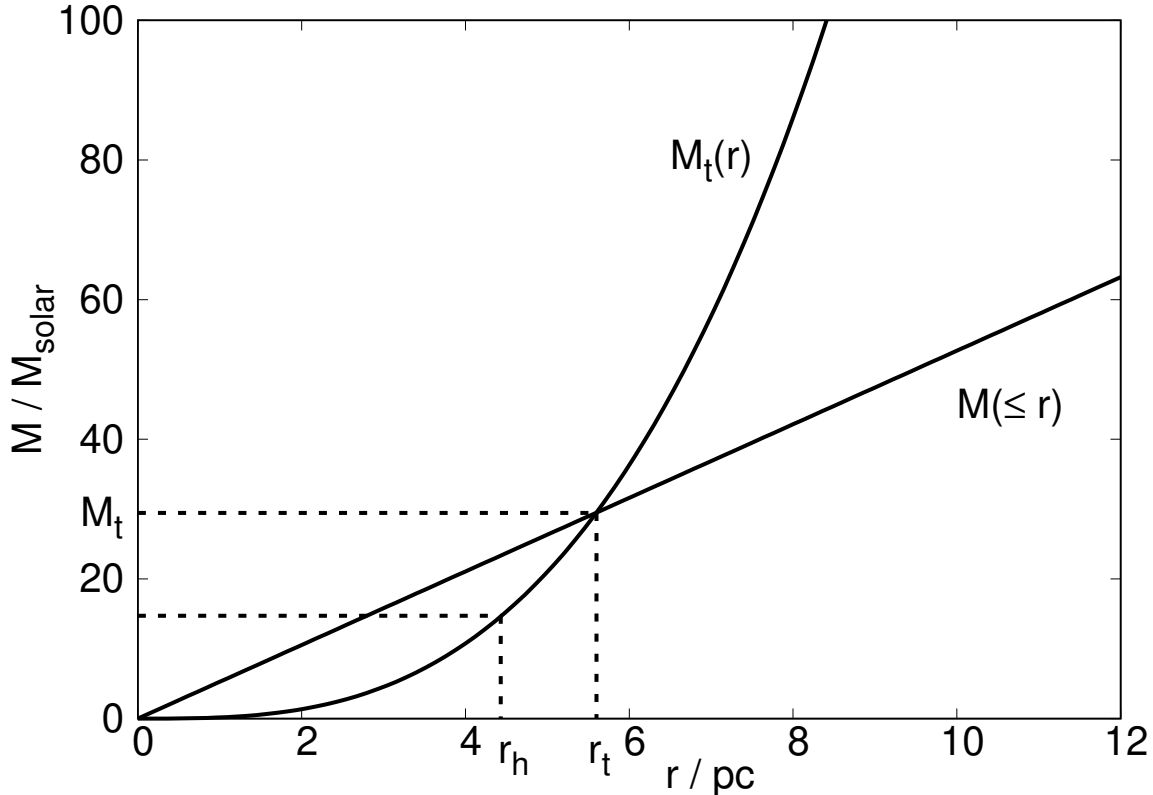


Figure 2. COIN-Gaia13: Observed radial cumulative mass distribution of stars in COIN-Gaia13, $M(\leq r)$ (as given by the data in Fig. 1), and the required tidal mass as a function of the radial distance to the cluster centre, $M_t(r_t)$ (Eq. 2).

$112 M_\odot$ (Coma Ber), while COIN-Gaia13 is derived here to weigh $M_{oc} = 29 M_\odot$. The CP method cannot assess ex-clusters stars beyond about d_{max} ahead or behind the clusters (for which the Jerabkova et al. 2021 CCP method is needed) and the star counts (n_l, n_t , respectively) are thus for the distance range between 10 pc and d_{max} (as listed in Table 1) ahead and behind the cluster. This distance range will be implemented in the models in Sec. 4. From the data in Table 1 we note that each of the six measurements has $n_l > n_t$.

As stars drift away from the open clusters, under- and over-densities along the star cluster tails form kinematically (Capuzzo Dolcetta et al. 2005). The existence and location of these under- and over-densities (see figs. 11 and 12 in Capuzzo Dolcetta et al. 2005) have been, later, also interpreted in terms of epicyclic motions relative to the centre of mass of the cluster (Küpper et al. 2008; Just et al. 2009). Overdensities of stars thus form at regular spacings ahead and behind the cluster, with Jerabkova et al. (2021) for the first time reporting evidence for their existence for an open star cluster. In Newtonian gravitation, the first epicyclic overdensities have a distance from the centre of mass position of the open cluster of $\Delta/\text{pc} \approx \pm 350 (M_{oc}/16400 M_\odot)^{1/3}$ (fig. 6 in Küpper et al. 2010) such that $\Delta \approx 64 \text{ pc}$ for

$M_{oc} = 100 M_\odot$ and $\Delta \approx 51 \text{ pc}$ for $M_{oc} = 50 M_\odot$, and are thus within the range $10 \text{ pc} - d_{max}$. In Newtonian gravitation, the overdensities and gaps are spaced symmetrically at equal distances from the cluster ahead and behind it (Capuzzo Dolcetta et al. 2005; Küpper et al. 2008; Just et al. 2009; Küpper et al. 2010), but in Milgromian gravitation the leading overdensity is at a larger distance from the cluster than the trailing one (Kroupa et al. 2022). This indicates that the escape speed is lower towards the leading tail such that stars escape slightly faster, and thus the relative spacing of the epicyclic overdensities is a sensitive measure of gravitational theory. For the purpose here, the number of stars in the leading and trailing tails, n_l, n_t , respectively, thus contains this information. If Newtonian gravitation were to be correct, then $n_l \approx n_t$ also because the leading and trailing Küpper epicyclic overdensities are symmetrically spaced relative to the cluster’s centre of mass position.

3. SYMMETRY ANALYSIS

If the four open clusters are orbiting in a smooth potential and are thus unperturbed then the stochastic Bernoulli calculation by Pflamm-Altenburg et al. (2023) can be applied to assess the likelihood of the observed n_l and n_t values to occur assuming the null hypothesis

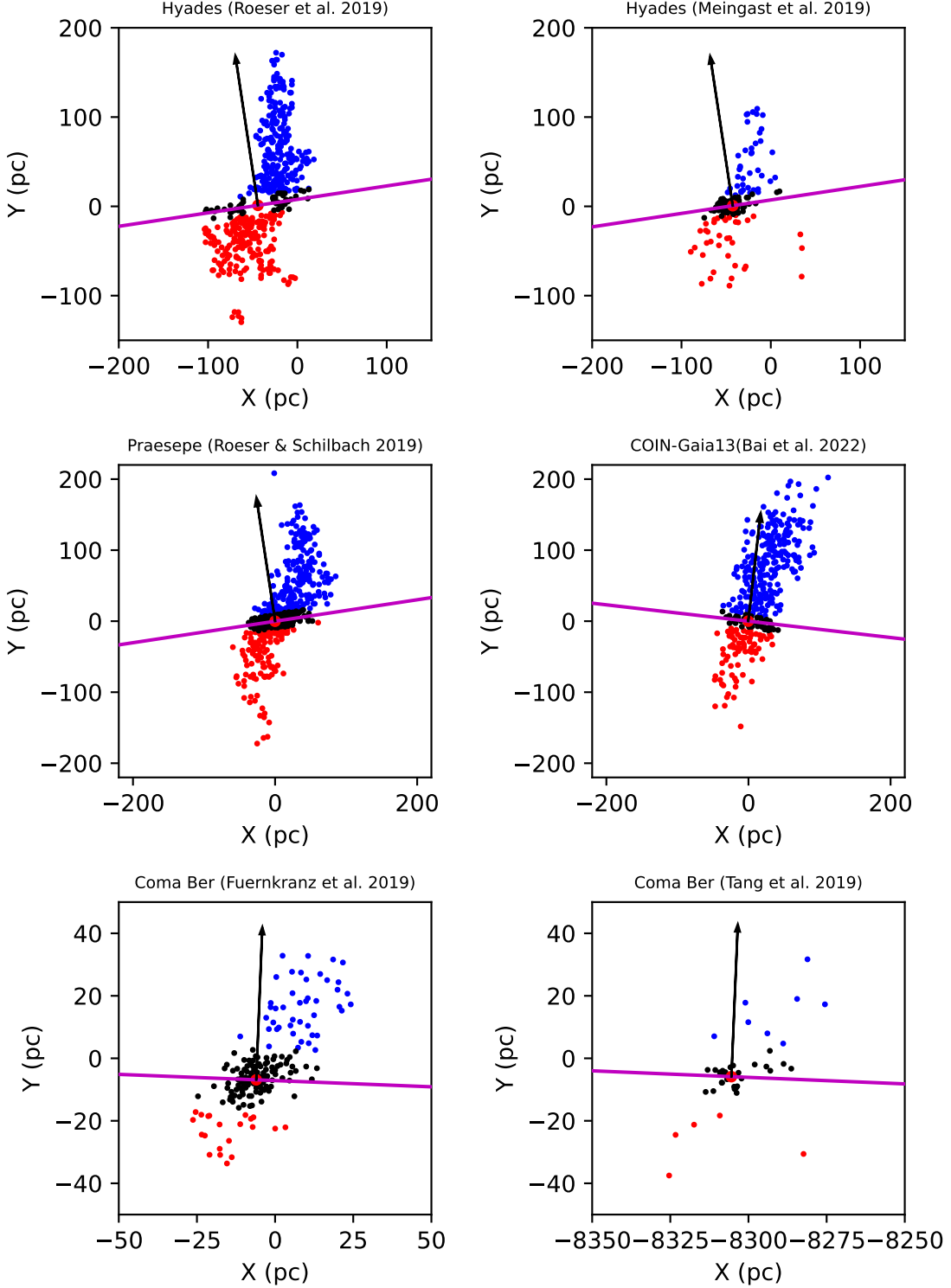


Figure 3. The ex-cluster star candidates in the leading tidal tail (blue) and trailing tidal tail (red) as obtained by the authors referenced at the top of each panel. In all panels, the centre of the open cluster is shown as the filled red circle, the Galactocentric motion vector of the cluster is shown as the black arrow and the line perpendicular to it passing through the cluster centre is the solid magenta line. Stars that are further from the magenta line than 10 pc in the leading tail sum up to n_l and stars in the trailing tail further than 10 pc from the magenta line sum up to n_t . The black stars are closer to the magenta line than 10 pc and are not used in the present analysis. The maximum distance, d_{\max} (Table 1), probed by the CP method in each case is given by the maximum extent of either the blue or red data clouds. *Upper left panel:* Hyades, as fig. 3 in Roeser et al. (2019). The X-anchor-point is the Sun. *Upper right panel:* Hyades, as fig. 3 in Meingast & Alves (2019). The X-anchor-point is the Sun. *Middle left panel:* Praesepe, as fig. 2 in Roeser & Schilbach (2019). The X-anchor-point is the cluster. *Middle right panel:* COIN-Gaia 13, as fig. 4 in Bai et al. (2022). The X-anchor-point is the cluster. *Lower left panel:* Coma Berenices, as fig. 2 in Fuernkranz et al. (2019). The X-anchor-point is the Sun. *Lower right panel:* Coma Berenices, as fig. 7 in Tang et al. (2019). The X-anchor-point is the Galactic Centre.

that Newtonian gravitation is valid. Following Pflamm-Altenburg et al. (2023), the normalised asymmetry parameter is defined as

$$\epsilon = (n_l - n_t) / (n_l + n_t). \quad (3)$$

This definition has the advantage that the quantity ϵ is symmetrical about 0. By the null hypothesis, the expectation value is $\mu_\epsilon = 0$ with variance $\sigma_\epsilon = 1/\sqrt{n}$. For each of the six measurements, the asymmetry significance $\sigma = |\mu_\epsilon - \epsilon|/\sigma_\epsilon$ is calculated and displayed in Fig. 4. For example, for the Hyades (Röser et al. 2019) the asymmetry significance is $\sigma = |0 - 0.12|/\sqrt{418} = 2.45$. The data for the Praesepe and for COIN-Gaia 13 constitute significant deviations from the null hypothesis, which is rejected with, respectively, 4.9σ and 8.39σ confidence.

Is it possible that Newtonian gravitation is valid but that the star counts and the application of the CP and CCP methods lead to a bias that creates a number asymmetry of the tidal tails? An interesting insight is obtained by the different teams reporting, for the same clusters, rather different numbers of tail members, despite using the same Gaia data releases (Table 1). This indicates the need to further study the tail-member extraction algorithms. Nevertheless, while the extracted numbers differ, in all cases the leading tail has more stars than the trailing tail. Particularly interesting is that the re-analysis by Thomas et al. (2023) of the Hyades using the CCP method but allowing the model cluster to evolve in non-axisymmetric Galactic potentials extracts different tail candidates than the original study by Jerabkova et al. (2021) who used an axisymmetrical potential. But both extracted tidal tails have comparable tail lengths and the asymmetry also remains similar. The clusters in Table 1 are in different directions as seen from the Sun, and this suggests that observational bias will not affect the star counts in the same manner. If such an effect were there, we might expect a more random result in terms of which half-tail contains more reported stars. Again, the finding that all measurements of all clusters available today indicate the same symmetry breaking suggests that an observational bias leading to this asymmetry is not likely.

Is it possible that Newtonian gravitation is valid but that the tidal tail asymmetries are a result of the open star clusters being perturbed? According to the data used here, the Praesepe and COIN-Gaia 13 show a very significant asymmetry (Fig. 4). This could be due to a perturbation. Indeed, Jerabkova et al. (2021) studied the possibility that the Hyades is heavily perturbed by a recent encounter which lead to the significant asymmetry of the number of stars in the leading and trailing

full-length tidal tails. A recent encounter with a massive perturber can lead to an effect comparable to the observed asymmetry of the full-length tidal tails, but the mass ($\approx 10^7 M_\odot$) and proximity (≈ 120 pc) appears for this to be unlikely because neither is a perturbation of the Solar neighbourhood field population known nor are there any correspondingly massive molecular clouds there, as pointed out by Jerabkova et al. (2021). The analysis here based on the inner tidal tail data as obtained by the CP method shows the Hyades to be consistent with the null hypothesis while the Praesepe (a 4.9 sigma deviation) and COIN-Gaia 13 (an 8.39 sigma deviation) are not. Combining the available information: The extended tidal tails of the Hyades are in > 5 sigma tension with the null hypothesis (Kroupa et al. 2022; Pflamm-Altenburg et al. 2023), and the inner tidal tails of the Praesepe are in 4.9 sigma and of COIN-Gaia 13 in > 5 sigma tension with the null hypothesis. The asymmetry is the same in all three cases, namely, the leading tail contains significantly more stars than the trailing tail. The remaining cluster, Coma Berenices, does not show a highly significant asymmetry but nevertheless also has $n_l > n_t$ at the near-3 sigma confidence level. While no perturber with a corresponding mass is evident to be present, the possibility that all of these clusters suffered an encounter at the same time leading to the same type of asymmetry appears to not be physically plausible.

4. MODELS

Sec. 3 documents that there is strong evidence that Newtonian gravitation may not be universally valid. In Sec. 4.1 Newtonian models of a Hyades-like cluster are studied to assess if a realistic orbit of an open cluster which includes passing through the Galactic mid-plane can lead to an asymmetry of its tidal tails. In Sec. 4.2 Milgromian- (MOND, Milgrom 1983; Famaey & McGaugh 2012; Milgrom 2014; Merritt 2020; Banik & Zhao 2022) and Newtonian-dynamics models are studied in order to advance our knowledge on the tidal tail asymmetry of open star clusters. We refer to Kroupa et al. (2022) for a thorough introduction and discussion of the problem.

4.1. Tidal-tail asymmetry due to Z-excursions?

Three Newtonian simulations (referred to in the following as models 1, 2 and 3 with different random number seeds for the stellar masses, position and velocity vectors but otherwise identical initial parameters) of a Hyades-like star cluster with an initial total mass of $1300 M_\odot$ and an initial Plummer parameter of $b = 2.3$ pc (half-mass radius of 3.0 pc) are performed to test if

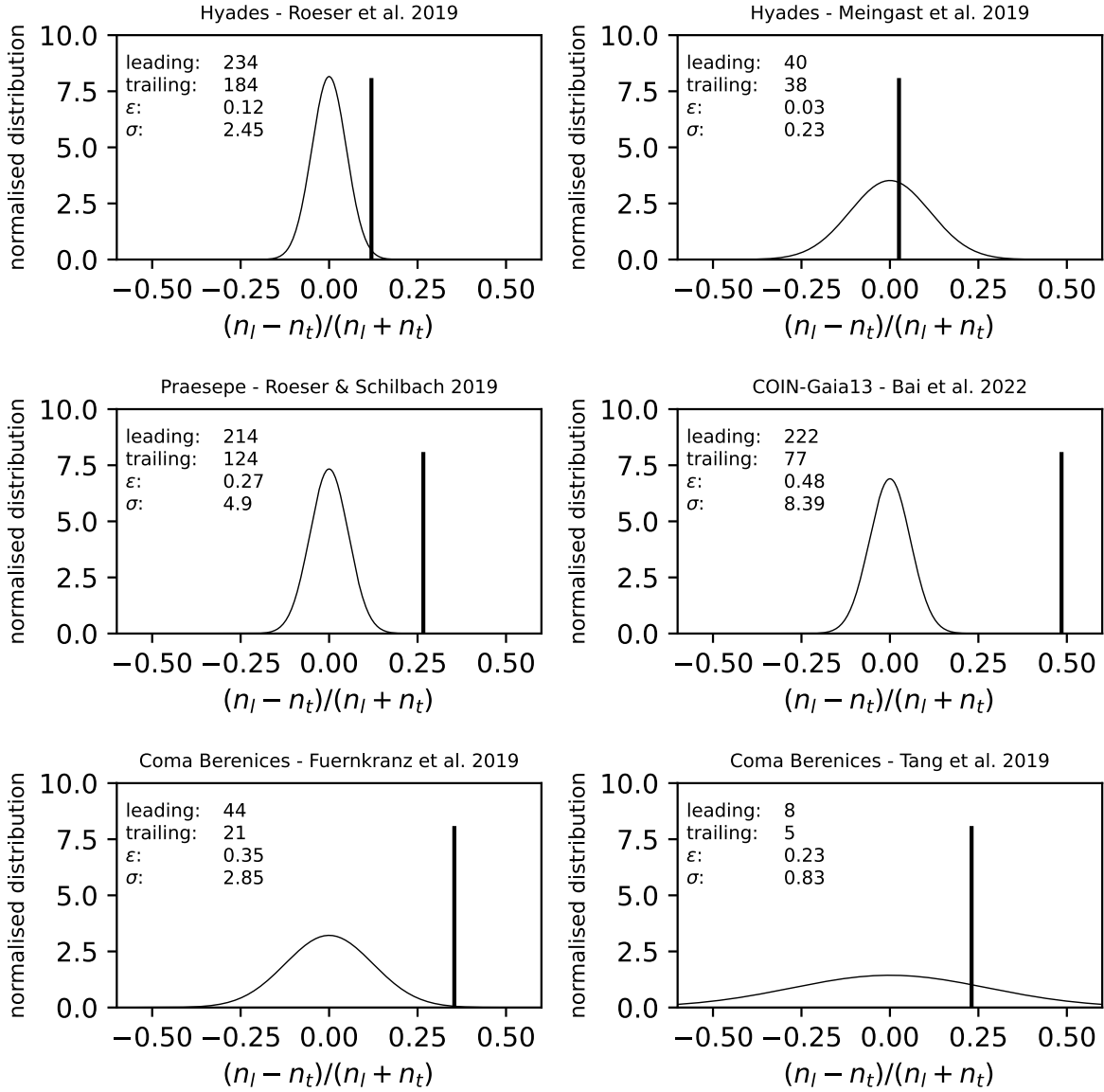


Figure 4. Application of the method of assessing the deviation from the null hypothesis in terms of σ for each of the six observations of tidal tails displayed in Fig. 3. The leading and trailing tail numbers for each observed tidal tail gauge the probability whether a measurement is one-sided asymmetric with $n_l > n_t$. See Sec. 3 for details.

a realistic Galactocentric orbit that is inclined to the Galactic plane might lead to periodic tidal tail asymmetries similar to those observed. The direct N -body code PETAR (Wang et al. 2020) is applied. It is a newly developed high-end code resting partially on the developments that lead to the Aarseth-suite of N -body models such as Nbody6 (Aarseth 1999, 2010). PETAR allows precise and accurate star–star force calculations and thus the integration of stellar orbits by being based on the Barnes-Hut tree method, the Hermite integrator and invoking slow-down algorithmic regularisation and thus also caters for high initial binary fractions.

The model clusters are initialised according to the Plummer phase-space distribution function (Plummer

1911; Aarseth et al. 1974). Modelling open star clusters with the Plummer phase space distribution function is motivated by its simplicity (e.g. Heggie & Hut 2003; Kroupa 2008) and Röser et al. (2011) and Röser & Schilbach (2019) finding it to match the observed density profiles of the Hyades and the Praesepe, respectively. The Plummer phase-space distribution function is also the simplest fully analytical solution of the stationary collision-less Boltzmann equation (e.g. Binney & Tremaine 1987).

The computations assume a canonical stellar IMF (Kroupa 2001) but no initial binary population, as these would significantly slow down the calculations without affecting the tidal tail symmetry. As Aarseth’s Nbody6

and Nbody7, PETAR incorporates stellar evolution using the updated single-stellar evolution/binary-stellar evolution (SSE/BSE) algorithms (Hurley et al. 2000, 2002; Banerjee et al. 2020). The Milky Way is modelled as an axisymmetric bulge+disk+dark halo potential as given by table 1 (MWPotential2014) in Bovy (2015). All clusters are initially positioned at coordinates corresponding to the Hyades, as detailed in Table 1 and the integrations of the stellar equations of motion extend up to 700 Myr.

The computations are conducted within a coordinate system that combines the Galactocentric system with a translation to the cluster’s center of mass. To align the model at any snapshot with a co-rotating frame, a rotational transformation along the Z -axis of this system is performed. This adjustment ensures that in the resultant $X - Y$ plane, the cluster consistently moves towards the positive Y -axis, with its center maintained at the origin. Tidal tail members are selected as stars in the leading tail that have a Y -coordinate ranging from +10 to +175 pc, and those from -175 to -10 pc as trailing tail stars (as for the Hyades, Table 1). Fig. 5 illustrates this approach to selecting tidal tail members at 200 Myr.

At the beginning of the calculations, the tidal tails are not yet formed. Consequently, to analyse the asymmetry, it is necessary to consider only the snapshots taken after a certain period. This determination is based on the scatter plots of stars for each model, akin to those illustrated in Fig. 5, but capturing various time points. Our analysis indicates that the tidal tails are well-developed by 200 Myr. Fig. 6 presents the evolution of the normalised asymmetry parameter ϵ (Eq. 3) in conjunction with the Z -position in the Galactocentric coordinate system. The findings demonstrate that excursions in the Z -position do not contribute to a positive ϵ . Further analysis on the significance of the asymmetry is shown in Fig. 7. For models 1 and 3, the significance consistently remains below $\sigma = 2$ once the tidal tails have formed. In contrast, model 2 exhibits its highest significance, nearly reaching $\sigma = 3$, at around 200 Myr. However, by 700 Myr, the asymmetry parameter ϵ becomes negative. No convincing correlation is evident between ϵ , σ and Z .

To avoid the stochastic effects stemming from model initialisation, the average number of stars in the leading and trailing tails are calculated at each snapshot by combining all three models. Fig. 8 displays the resulting asymmetry parameter, ϵ , and its significance, σ . The asymmetry parameter indicates a positive asymmetry, meaning the leading tail consistently contains more stars than the trailing tail. However, the significance of this finding is minimal, remaining below $\sigma < 1.7$.

A significant correlation with Z is not apparent in the model-averaged values of ϵ and σ .

In conclusion, a realistic orbit of an open cluster oscillating about the mid-plane of the Galactic disk therefore does not lead to a significant ($\sigma > 3$) asymmetry of the tidal tails. Thus Milgromian models are considered next in comparison to Newtonian models computed with the new MLD N -body code.

4.2. MOND and the MLD code

MOND is a non-relativistic theory that generalises Newtonian gravitation and is non-linear such that the potential around an open star clusters near the Solar circle is asymmetrical. In particular, fig. 3 in Kroupa et al. (2022) explains why a Milgromian star cluster loses more stars per unit time into the leading tail than a Newtonian star cluster. First of all, in Newtonian gravitation the restoring force towards the star cluster’s centre is equal and opposite on opposing sides of the cluster’s centre such that both tails are fed equally by evaporating stars. In contrast, in Milgromian dynamics, the potential of the cluster on the side towards the Galactic centre has a reduced restoring force by about 15 per cent (for the point-mass approximation shown in fig. 3 in Kroupa et al. 2022) towards the cluster than the backwards side such that more stars can exit it thus ending up in the leading tail which is fed by stars falling towards the Galaxy’s centre. The fractional reduction of the restoring force however depends on the mass and extent of the open cluster and on the particular formulation of MOND used – see below – and needs further theoretical and empirical exploration. It is also possible that the escape speeds are very similar but that the práh on the Galactic near side has a larger extent than the práh at the far side such that more stars can escape towards the Galaxy. Investigations are on-going as to the details of stellar escape in Milgromian dynamics. Kroupa et al. (2022) demonstrated that this práh asymmetry leads to the type of asymmetry detected here, namely that the leading tidal tail of a star cluster has, most of the time, more stars than the trailing tail. Those models concentrated on the full extent of the tidal tails in comparison with data extracted using the CCP method, and the models were idealised by the clusters being set-up on circular mid-plane orbits in the Galactic disk. Here realistic orbits are studied considering tidal tail data extracted using the standard CP method which means only the tidal tails near to the cluster are assessed (Sec. 2). Discussed next, there are three different formulations of MOND as a gravitational theory that allow the integration of the equations of motion of particles in a force-field gener-

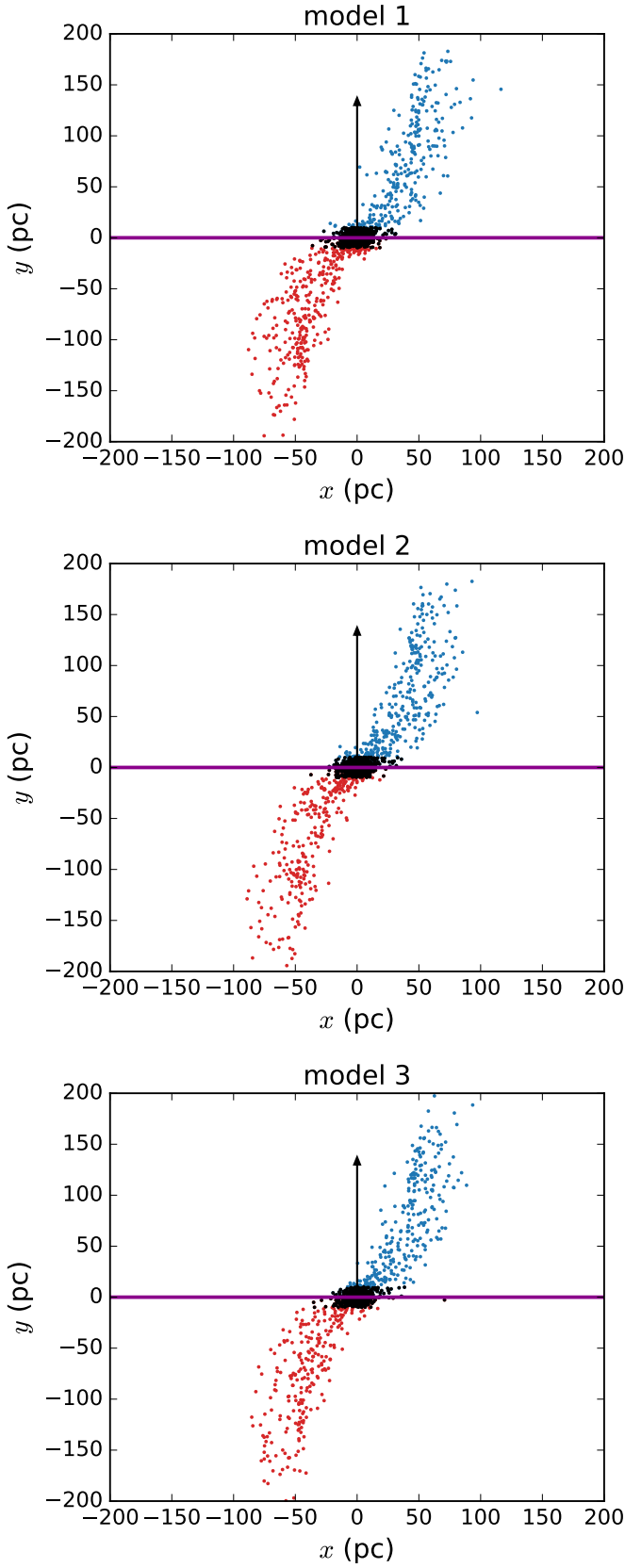


Figure 5. Calculated Newtonian Hyades-like models at 200 Myr. Black dots represent non-tidal tail stars. Blue dots and red dots denote stars in the leading and trailing tails, respectively. Black arrows show the Galactocentric motion vector of the cluster and the line perpendicular to it passing through the cluster centre is the solid magenta line. We show model 1, 2 and 3 from the top to the bottom panels. Note that $x = X, y = Y$ (see text).

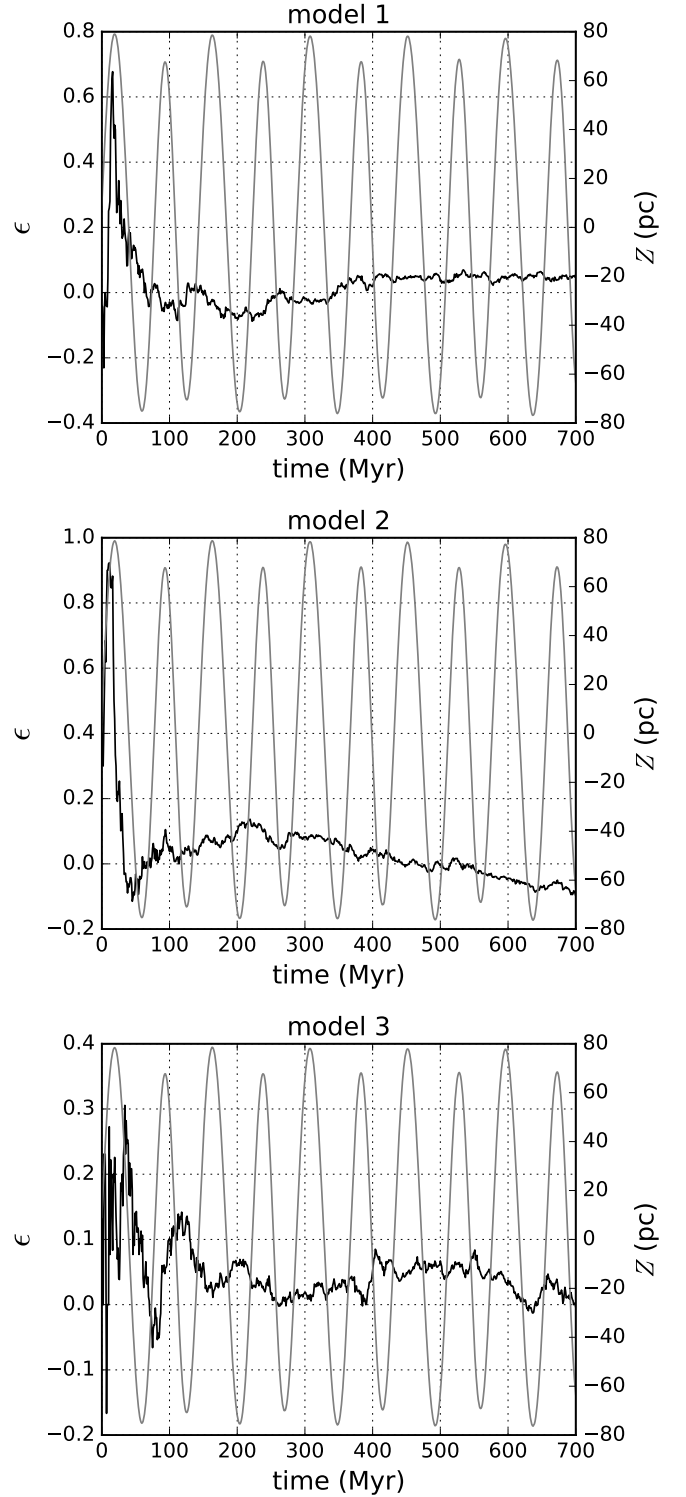


Figure 6. The solid black lines show the time evolution of the normalised asymmetry parameter ϵ (Eq. 3) for the Newtonian models of Sec. 4.1. In each panel, the grey line is the Z -position at each time point. Model 1, 2 and 3 are shown from the top to the bottom panels. Note that at the begin of the calculation, the tidal tails are not formed, the results before ≈ 200 Myr therefore not no being reliable.

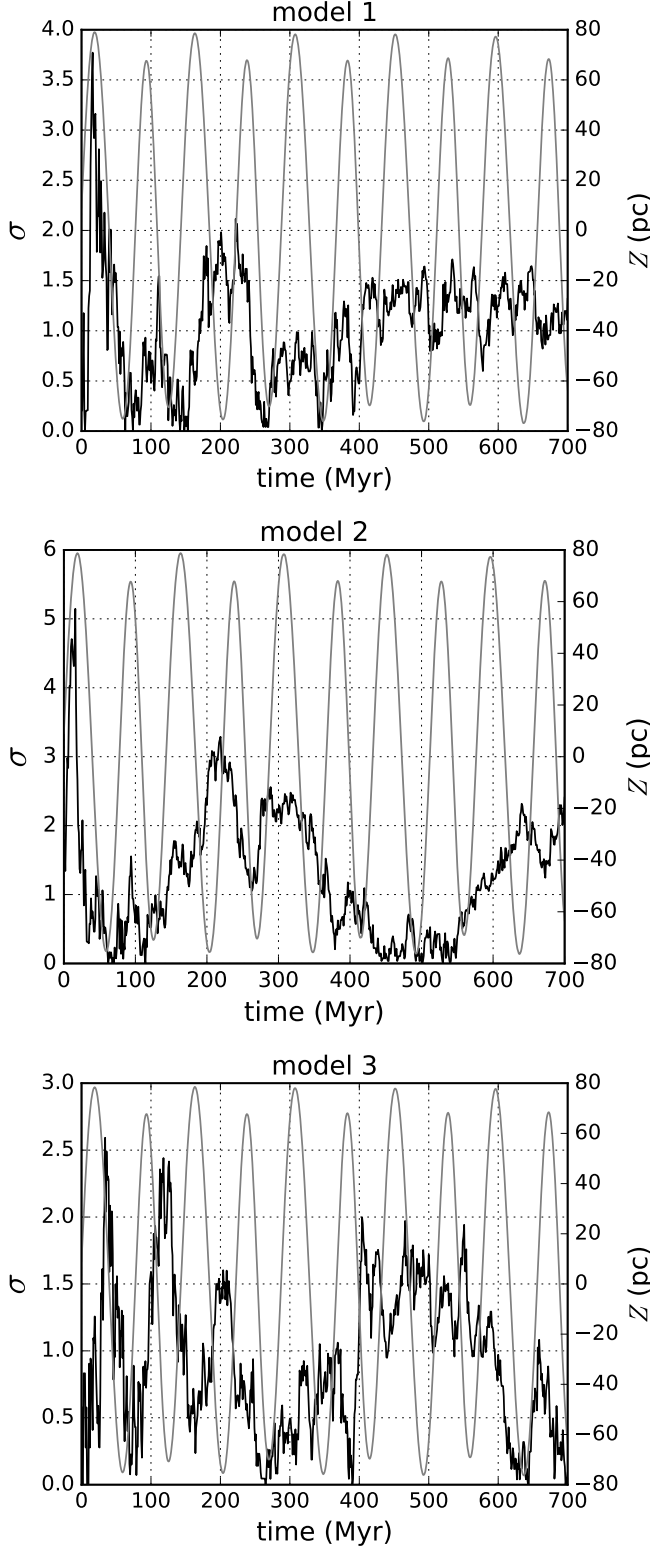


Figure 7. The solid black lines show time evolution of the asymmetry significance, σ (Sec. 3) for the Newtonian models of Sec. 4.1. The grey line in each panel shows the Z -position at each time point. Otherwise as Fig. 6.

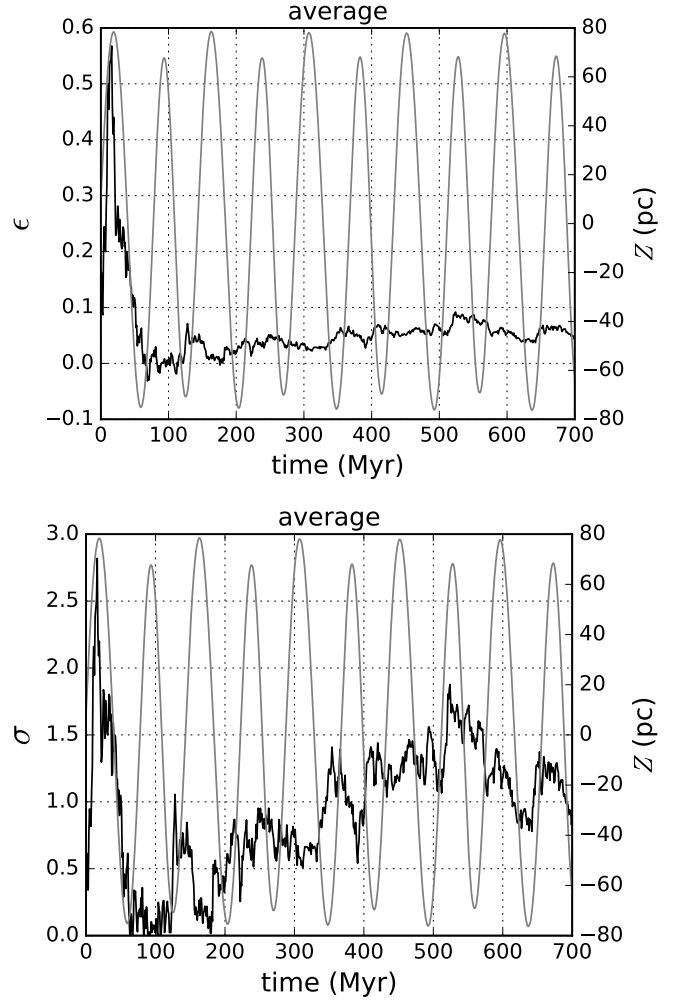


Figure 8. The averaged normalised asymmetry parameter (left, solid line, Eq. 3) and averaged asymmetry significance (right, solid line, Sec. 3) for the combined three Newtonian Hyades-like models of Sec. 4.1. In each panel, the grey line is the averaged Z -position for the three models 1, 2 and 3. Note that there is no significant correlation between ϵ and σ with Z and that $\sigma < 1.7$ for $T > 200$ Myr in agreement with the computational results using the MLD code in Newtonian mode of Sec. 4.2.

ated by the matter distribution: AQUAL (Bekenstein & Milgrom 1984), QUMOND (Milgrom 2010) and MLD (Pflamm-Altenburg 2024). AQUAL and QUMOND are field-formulations relating the true (Milgromian) gravitational field, Φ , to its source, the baryonic matter distribution, ρ . MLD is a particle-based formulation and rests on calculating the particle forces directly.

Very briefly on AQUAL: consider the following quasi-linear elliptic partial differential equation of second order where the left hand side is the p-Laplace operator with $u = \Phi_p/a_0$ being the generalised potential with unit of length, $\vec{\nabla} \cdot [|\vec{\nabla} u|^{p-2} \vec{\nabla} u] = 4\pi G \rho/a_0$. It can

be seen that for $p = 2$ the standard Poisson equation is obtained with the matter density ρ sourcing the (Newtonian) potential $\Phi_{p=2}$. For $p = 3$, ρ sources the non-Newtonian potential $\Phi_{p=3}$. In both cases the negative gradient, $-\vec{\nabla}\Phi_p$, is the acceleration. The $p = 3$ case corresponds to the deep-MOND limit where the equations of motion are space-time-scale invariant (Milgrom 2009). The full description includes the transition from the $p = 2$ to the $p = 3$ Laplace operator when $|-\vec{\nabla}\Phi| \approx a_0 \approx 3.9 \text{ pc/Myr}^2$ with $\Phi = \Phi_{p=2}$ when $|-\vec{\nabla}\Phi| \gg a_0$ and $\Phi = \Phi_{p=3}$ when $|-\vec{\nabla}\Phi| \ll a_0$. It can be formulated in terms of a Lagrangian (Bekenstein & Milgrom 1984). The transition of non-relativistic dynamics away from Newtonian dynamics to Milgromian dynamics may be due to the quantum vacuum (Milgrom 1999). Relativistic formulations that encompass these non-relativistic field equations have been developed (see Banik & Zhao 2022 for a review). In Kroupa et al. (2022) the related Lagrangian-based quasi-linear formulation of MOND (QUMOND) was applied to do the simulations because it is computationally more efficient. QUMOND rests on the idea that the Newtonian potential generated by ρ can be augmented by a phantom dark matter potential (which does not consist of real dark matter particles) such that the combination of both potentials yields the total Milgromian potential. The AQUAL and QUMOND formulations of MOND differ when $|-\vec{\nabla}\Phi_p| \approx a_0$ and this regime is also sensitive to the transition function between the $p = 2$ and the $p = 3$ regimes. By choosing to use QUMOND and a particular transition function, Kroupa et al. (2022) explored the general effect of MOND on the escape of stars across the práh of their cluster. However, this approach becomes untenable to model the low-mass open clusters in Table 1. Numerical simulations of stellar dynamical systems by use of field theoretical descriptions require a sufficiently smooth mass density distribution. QUMOND simulations show that the dynamical evolution of already intermediate mass star clusters ($\approx 5000 M_\odot$) is effected by the limitation of the grid resolution and the graininess of the gravitational potential (Kroupa et al. 2022). Therefore, the self-consistent simulation of star clusters with smaller masses require direct N -body methods in a MONDian context. The above non-linear MONDian field equations have not yet been discretised such that an N -body code has, until now, not been available to study the dynamical evolution of open star clusters.

In *Milgromian Law Dynamics* (MLD), and as a first step towards such a MOND N -body code, Milgrom’s law (Milgrom 1983) is postulated to be valid in vectorial

form (Pflamm-Altenburg 2024),

$$\mu(a_i/a_0) \vec{a}_i = \vec{g}_i, \quad (4)$$

which connects the kinematical acceleration of star i , \vec{a}_i ($a_i = |\vec{a}_i|$), to its formal Newtonian gravitational acceleration, \vec{g}_i . The acceleration \vec{g}_i of each particle is obtained from the sum of the Newtonian gravitational forces from all other particles, just as in standard Newtonian N -body codes (e.g. Aarseth 1999; Wang et al. 2020). The acceleration, $\vec{a}_{G,i}(\vec{D}_i)$, acting on particle i from the full Galactic potential at the particle’s location, \vec{D}_i , is added vectorially to \vec{g}_i . The transition function has the property $\mu \rightarrow 1$ for $a_i \gg a_0$ and $\mu \rightarrow a_i/a_0$ for $a_i \ll a_0$ such that Newtonian dynamics is obtained in the former case (e.g. in the planetary-regime of the Solar system). The standard transition function, $\mu(x) = x / (1 + x^2)^{1/2}$ (Famaey & McGaugh 2012), is applied here. The external field effect (EFE), a unique new physical phenomenon in MOND and non-existent in Newtonian dynamics (e.g. Haggi et al. 2016; Chae et al. 2020, 2021; Chae & Milgrom 2022), is taken into account automatically in MLD because the transition function μ is on the left-hand side of Eq. 4. The MLD code is published by Pflamm-Altenburg (2024) where detailed tests are documented and conserved quantities are derived.

In the MLD code, the standard Hermite scheme used in direct N -body codes (Hut et al. 1995; Makino 1991; Kokubo et al. 1998; Aarseth 1999, 2010) is implemented to integrate the equations of motion of the stellar particles using the accelerations and jerks in a predictor-corrector method. The MOND-accelerations, \vec{a}_i , are obtained by solving Eq. 4, and the corresponding jerks are calculated as the time derivative of the accelerations. In order to avoid the Newtonisation of the centre of mass of the star cluster in this MOND formulation and to avoid the handling of rare but computationally-intensive close encounters, the gravitational N -body force has been softened (Aarseth 1963). Here, a softening parameter $\varepsilon = 0.1 \text{ pc}$ is used. This softening does not allow a realistic assessment of the true evaporation rate which is driven by the two-body relaxational process. It avoids excessive computational time but allows the softened particles to self-consistently generate the Milgromian or Newtonian potentials and thus to map out the directionality of the relative mass loss from the cluster. In this sense the MLD code is a first step akin Aarseth (1963) in the Newtonian case and will be developed further by including regularisation methods as well as stellar and binary-star evolution algorithms. The simulations in pure Newtonian dynamics are performed with the same MLD code with the same softening by setting the threshold acceleration to $a_0 = 3.9 \times 10^{-20} \text{ pc/Myr}^2$.

To model the open clusters in Table 1 using the MLD code, first their initial positions in the Galaxy need to be obtained by backwards integration to then forward-integrate the initialised cluster to its presently observed position. Thus the present-day position of the star cluster centre is calculated backward in time for a time equal to the mean estimated age \bar{T} (same procedure as used in Kroupa et al. 2022). At this position a Plummer phase-space distribution function is set up as in Sec. 4.1 with an initial Plummer parameter b as in Table 1 and containing $N = 2000$ particles of equal mass $m_i = 0.5 M_\odot$. In the case of the simulations of COIN-Gaia13, $b = 3.4$ pc and the particle number is $N = 500$ with a total mass of $439 M_\odot$ (Sec. 2) in order to reach the dissolved state of this cluster.

In the next step each particle i in the star cluster is integrated forward in time using the MLD code. All particles are kept in the calculation, and a spherical logarithmic Galactic gravitational potential, $|\bar{a}_{G,i}| = V_c^2 / (X_{G,i}^2 + Y_{G,i}^2 + Z_{G,i}^2)^{1/2}$, is used. It corresponds to a flat rotation curve of $V_c = 225$ km/s, with $X_{G,i}, Y_{G,i}, Z_{G,i}$ being the Galactocentric Cartesian coordinates of particle i . The calculation proceeds until the density centre of the star cluster comes closest to the current position of the observed star cluster. The Solar position in this coordinate systems is $X_{G\odot} = -8300$ pc, $Y_{G\odot} = 0$ pc, $Z_{G\odot} = 27$ pc. The position of the density centre of each model is found by calculating the density-weighted radius based on the innermost 20 per cent of particles (Casertano & Hut 1985; Heggie & Aarseth 1992; Kroupa et al. 2001). At this point the model cluster has a very similar position relative to the Sun and its tidal tails are extracted just as for the observed clusters in Sec. 2. In order to obtain sufficient statistics of the tail occupation numbers, for each of the observed star clusters listed in Table 1 three models with different initial random number seeds are calculated in MLD and in Newtonian dynamics.

5. RESULTS

5.1. The observed clusters

In Sec. 3 the asymmetry-significance, i.e. the probability of obtaining the number of stars in the leading and trailing tails, was computed for each observational study of the four open clusters listed in Table 1, the results being documented in Fig. 4. In order to assess the probability whether the combined data of the clusters are consistent with the null hypothesis (symmetrical tails, i.e. Newtonian dynamics is valid) the observed cluster data are stacked. Since the escape of stars under the null hypothesis can be very well described as a stochastic process (Pflamm-Altenburg et al. 2023) we can add

the leading and trailing tails in the observed clusters (Fig. 3), $n_{l,\text{sum}} = \sum_{i=1}^6 n_{l,i}$ and $n_{t,\text{sum}} = \sum_{i=1}^6 n_{t,i}$. This combined data set is extremely significantly discrepant with the null hypothesis because the available measurements of the tidal tail membership have significantly more stars in the leading than in the trailing tail. Based on the observational data, the null hypothesis is therefore rejected with 8.99σ confidence (Fig. 9).

5.2. The models

The above asymmetry-significance is also calculated for each of the models in order to assess if these confirm the rejection: Are the tidal tails of the Milgromian models as asymmetric as the observed ones? And do the Newtonian models confirm the expected symmetry (Pflamm-Altenburg et al. 2023)?

As described in Sec. 4, for each open star cluster in Table 1 three models are computed with the MLD code in each of the gravitational theories in order to improve the statistics in the model data. The final snapshots, when the respective model is at the position of the observed cluster, are stacked and shown in Fig. 10–11.

The distribution of particles on the sky of the stacked models are shown in Fig. 12 to illustrate the sky-position, size and extent of the tidal tails of each of the open star clusters in Table 1. It is evident that the Milgromian and Newtonian models look, at first sight, similar. More subtle differences can be seen in the case of Coma Ber which is a close-by old cluster close to disruption (the Praesepe has a similar age and contains significantly more stars, Table 1).

The probabilities that the individual stacked models are consistent with the null hypothesis are evaluated next. The numbers of particles and probabilities are shown in Fig. 13. It is already readily apparent, by comparing with the observed clusters (Fig. 4), that the Milgromian models are indeed highly inconsistent with symmetric tails, the leading tail always containing significantly more stellar particles than the trailing one. The Newtonian models, on the other hand, confirm these to be consistent with symmetrical tidal tails. In order to assess the overall probability that Milgromian or Newtonian models are consistent with the null hypothesis, all Milgromian and Newtonian models are stacked into one respective representation, as done for the observed clusters (Fig. 9). As shown in Fig. 14, the Milgromian models are consistent with the observed tails by both being significantly dislodged from the normalised probability distribution, while the Newtonian ones are well consistent with this distribution. Thus, the Newtonian models computed with the MLD code confirm that Newtonian tidal tails are symmetrically occupied, while the

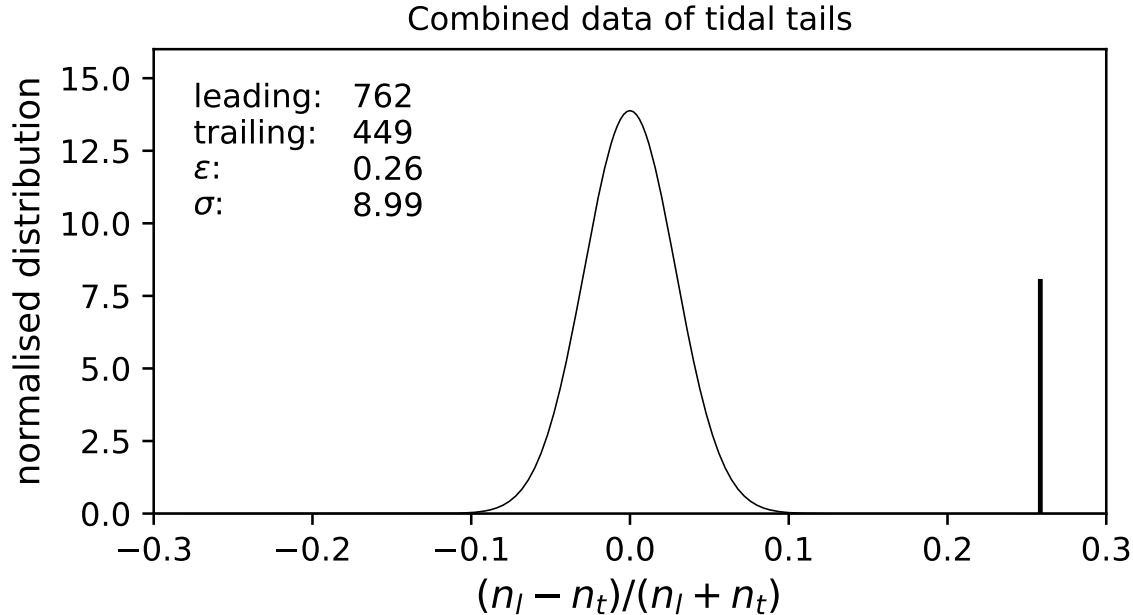


Figure 9. As Fig. 4, but here the number of stars in the leading and trailing tails are combined from all observed tidal tails to assess the probability whether all measurements are one-sided asymmetric with $n_{l,\text{sum}} > n_{t,\text{sum}}$.

Milgromian computations with this same code confirm the MOND-asymmetry already noted by Kroupa et al. (2022) on the basis of a QUMOND code. The combined Milgromian models indeed show a comparable asymmetry significance (8.63σ , Fig. 14) as the combined observed clusters (8.99σ , Fig. 9). Interesting to note is also that the combined Milgromian models have $n_M = 411$ particles in the leading and trailing tails, while the Newtonian models have $n_N = 385$ such particles. The difference, $n_M - n_N$, corresponds to a three-sigma effect that suggests Milgromian open clusters to dissolve more rapidly than equivalent Newtonian ones as discussed in Kroupa et al. (2022). This may be one reason why observed open star clusters are found to be dissolving more quickly than expected from Newtonian N -body models (Dinnbier et al. 2022).

The four observed open star clusters that have tidal tail data thus appear to compellingly indicate Milgromian rather than Newtonian gravitation to be the valid description of gravitational dynamics on the pc-scale.

6. CONCLUSIONS

The tidal tails of open star clusters near to the Sun allow to test gravitational theory. The leading and trailing tails have, within statistical uncertainties, the same number of stars if Newtonian gravitation is valid. If Milgromian gravitation is valid, then the leading tail will have significantly more stars than the trailing tail. We use the data from six teams that had extracted tidal tail

candidate stars for the four nearby open star clusters Hyades, Praesepe, COIN-Gaia13 and Coma Berenices using the standard CP method that allows to find co-moving ex-cluster member stars still in the vicinity of an open star cluster. The available data reject Newtonian symmetry with 8.99σ confidence, but are well consistent with Milgromian gravitation.

The Milky Way’s bar potential cannot produce this asymmetry (Rossi & Hurley 2015; Thomas et al. 2023), and encounters with massive structures also cannot simultaneously account for the similar asymmetries observed in open star clusters that are at different locations around the Sun. Newtonian simulations performed here show that a Hyades-like cluster which periodically oscillates through the Galactic disk over 700 Myr never shows a significant asymmetry as a consequence of the disk crossings. While star-cluster simulations in Newtonian gravitation cannot explain this asymmetry, simulations in Milgromian gravitation naturally produce the observed asymmetry. Further tidal-tail data are needed for confirmation and additional Newtonian modelling is required including perturbations of the Milky Way potential through its spiral arms (Thomas et al. 2023) to sharpen these results.

The Milgromian and Newtonian N -body computations presented here support Milgromian open clusters to be dissolving more rapidly than their Newtonian counterparts, and the present analysis finds the open

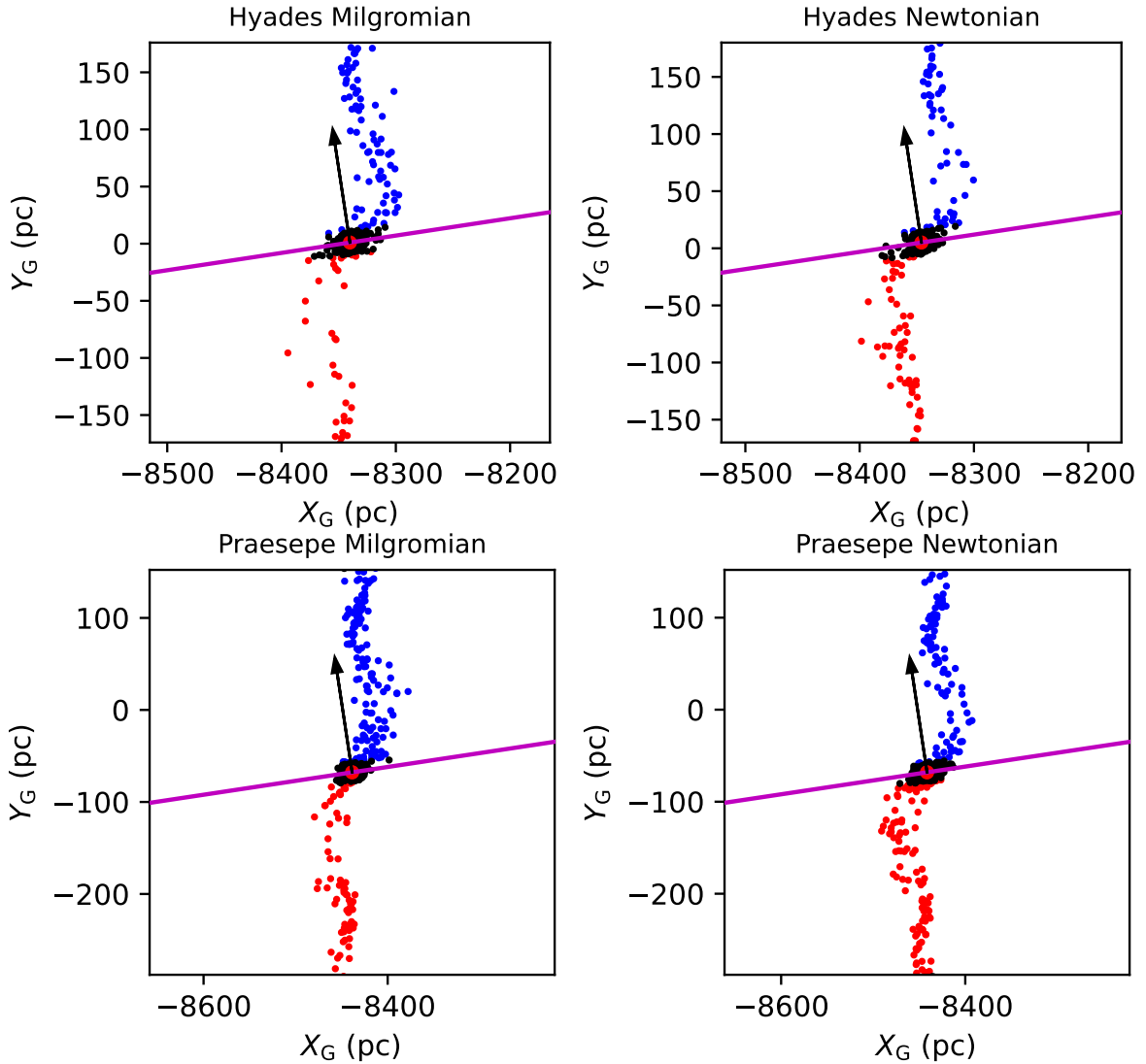


Figure 10. Star cluster models: The three stacked Milgromian (left) and three stacked Newtonian (right) models stellar-dynamically evolved with the MLD code (Sec. 4). The models are at the same location relative to the Sun as the real cluster and the symbols and spatial scales are as in Fig. 3 From top to bottom: Hyades, Praesepe.

cluster COIN-Gaia13 to be nearly completely dissolved. Open star clusters near the Galactocentric distance of the Sun are strongly subject to the EFE because the external field from the Galaxy is comparable to a_0 and the internal acceleration of the open clusters is much smaller than a_0 (Kroupa et al. 2022). The results here suggest MOND rather than Newtonian dynamics to be relevant for understanding the dynamical evolution of open star clusters. But the relatively modest available data requires a significant further effort on obtaining more tidal tail data in conjunction with computer modelling in order to constrain the correct formulation of Milgromian dynamics and the transition function. Additional tidal tail data will become available for open star clusters at larger distances from the Sun than the currently available clusters. Open clusters that are ahead of the Sun

in terms of Galactic rotation will allow Gaia data to assess their trailing tails with more accuracy and precision than the leading tails, while open clusters behind the Sun will allow a more accurate and precise mapping of their leading arms than their trailing arms. This leads to a bias that needs to be catered for in the tail-symmetry analysis.

Placing the above findings into a broader context, is Milgromian dynamics relevant beyond open star clusters? The Hubble Tension has been shown to be resolved by galaxies falling in a Milgromian gravitational field to the sides of a Gpc-sized local void we are in, a void that is not possible in the standard dark-matter-based cosmological model but readily forms in a MOND cosmological model (Haslbauer et al. 2020; Mazurenko et al. 2024).

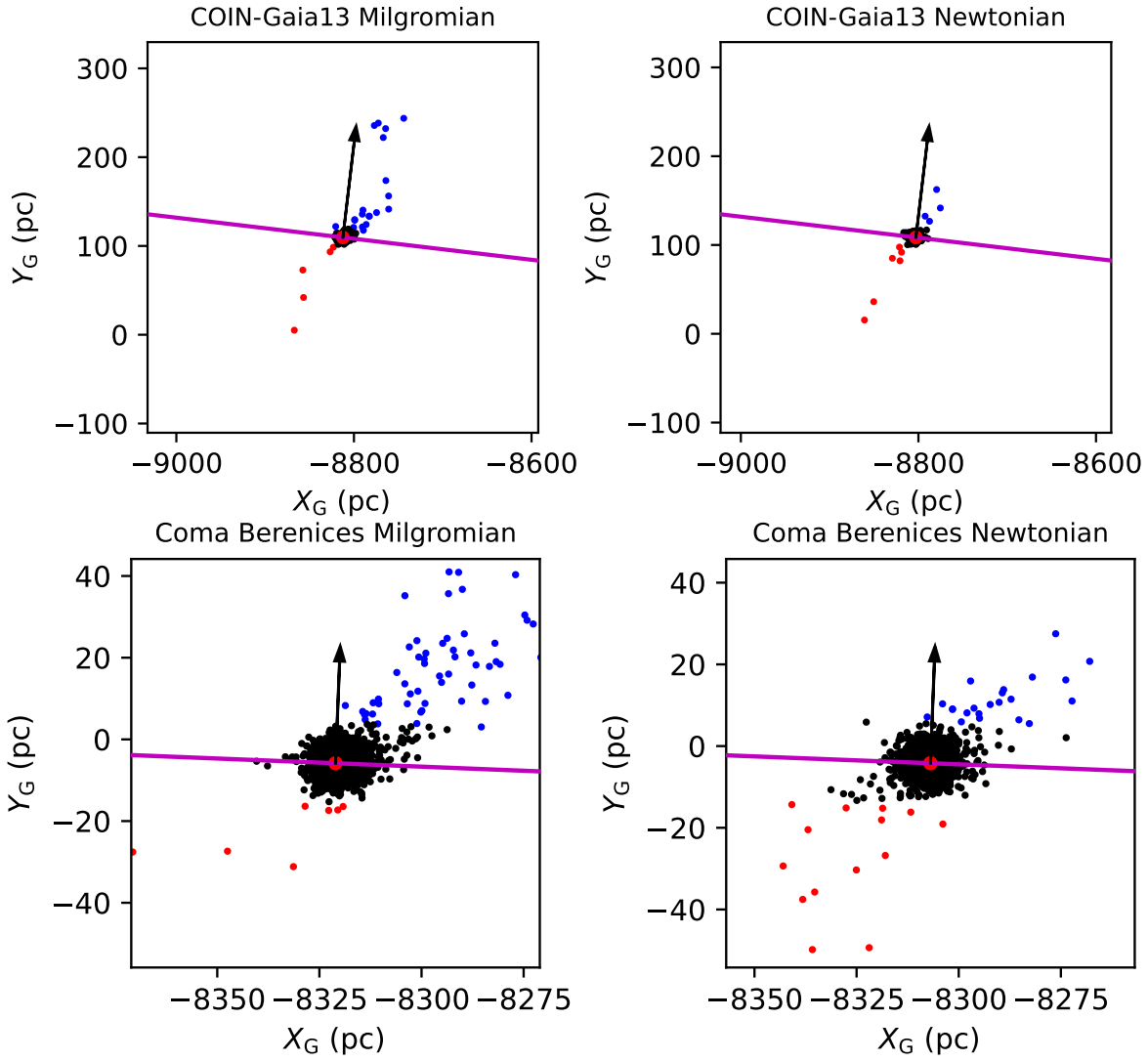


Figure 11. As Fig. 10 but for COIN-Gaia13, Coma Berenices.

Galaxy clusters have been posing some tension in that a factor of two in mass appears to be missing but can be accounted for in MOND if sterile neutrinos exist (e.g. Banik & Zhao 2022 and references therein) and also if appropriate boundary conditions are taken into account for these large structures (López-Corredoira et al. 2022). The prominent Bullet cluster of galaxies has been used as a default object for the proof of the existence of dark matter particles. But the fulfilment of hydrostatic equilibrium required for the mass determination of the hot gas seems to be problematic (Pflamm-Altenburg 2024). Problems of explaining the Bullet (and the El Gordo) galaxy clusters in the standard Λ CDM cosmological model of structure formation have been noted. These galaxy clusters are, however, well understood in a Milgromian cosmological model (Kraljic & Sarkar 2015; Asencio et al. 2021, 2022).

It is already well established that Milgromian gravitation correctly accounts for the properties of elliptical galaxies (Eappen et al. 2022; Eappen & Kroupa 2024), and of disk galaxies (e.g. Famaey & McGaugh 2012; Banik & Zhao 2022; specific example: M33, Banik et al. 2020; natural formation of exponential disk galaxies: Wittenburg et al. 2020; star-formation properties: Nagesh et al. 2023). The availability of Gaia DR3 has allowed independent teams to assess the rotation curve of the Galaxy at Galactocentric distances of 19 to 27 kpc. Sylos Labini et al. (2023); Jiao et al. (2023); Wang et al. (2023) and Ou et al. (2024) all find it to be decreasing over this distance range by about 30 km/s being consistent with a Keplerian decline. While a flat MONDian rotation curve is rejected with 3σ confidence by Jiao et al. (2023), Ou et al. (2024) stress that globular clusters and satellite galaxies lead to significantly higher rotation speeds at distances from ≈ 15 to ≈ 200 kpc. The Kep-

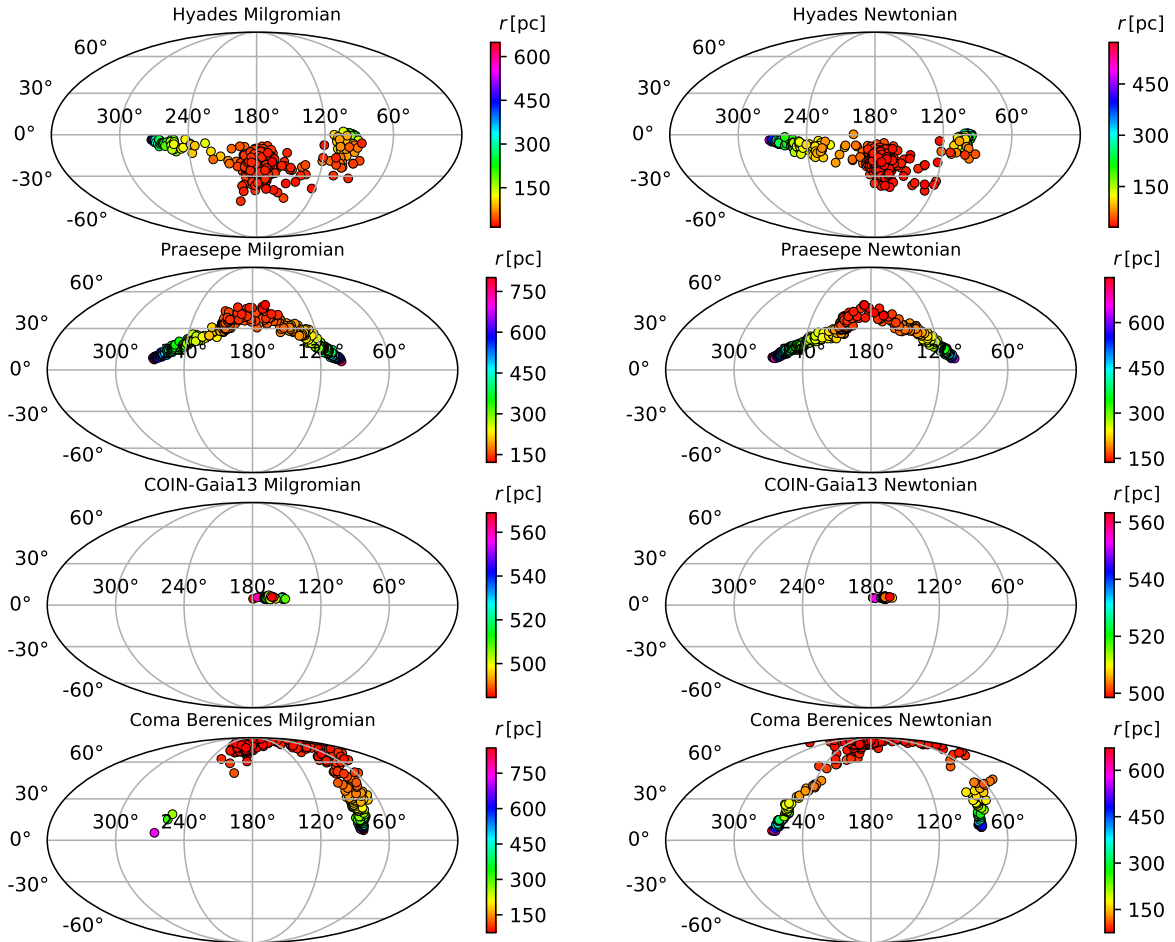


Figure 12. The three stacked Milgromian/Newtonian models of the clusters shown in Fig. 10–11 are presented here in full length as they appear on the model sky in Galactic longitude and l and latitude b , where $l = 0^\circ, b = 0^\circ$ is the direction towards the Galactic centre. The left panels are the Milgromian models and the right panels the Newtonian ones. The colour of a stellar particle indicates the distance as indicated in the key. As the Galaxy is rotating in clockwise direction the leading tails are here on the right of the star clusters.

lerian fall-off between ≈ 19 and ≈ 27 kpc is associated with divergent stellar radial velocity components (fig. 8 in Wang et al. 2023) which compromises simple solutions of the Jeans equation and suggests a strongly perturbed outer Galactic disk. The Keplerian fall-off is also associated with a break of the stellar surface density at about 17 kpc with a steep radial decline to larger Galactocentric distances (fig. 4 in Sylos Labini et al. 2023). This feature is very similar to such a break at 20 kpc and similar decline of the disk surface density in Milgromian models of the Galaxy that involve an encounter with Andromeda ≈ 10 Gyr ago (fig. 3 in Bílek et al. 2018). Such Milgromian models of the dynamical history of the Local Group need more exploration for the exact timing, close-encounter distance and initial galaxy configurations (e.g. radii and masses of the pre-encounter galactic disks). But we already know that they naturally explain the observed thin/thick disk components, warps of the Milky Way and of Andromeda disks, the planar satellite galaxy

arrangements around both of them, while also being consistent with the present-day inclinations of the Galactic and Andromeda stellar and gaseous disks as well as their relative distance and velocity of approach (Bílek et al. 2018; Banik et al. 2022).

Recent work on dwarf spheroidal satellite galaxies (Safarzadeh & Loeb 2021) reports difficulties in matching their kinematical data by MOND. This problem remains unsolved in Milgromian dynamics needing attention, but does not imply that Newtonian solutions with dark matter exist (e.g. Kroupa 1997; McGaugh & Wolf 2010).

On the scale of thousands of AU, the very-wide-binary-star test has been shown to falsify Newtonian dynamics with the data being consistent with Milgromian dynamics (Hernandez et al. 2012, 2019, 2022; Chae 2023; Hernandez 2023; Hernandez et al. 2024; Chae 2024). Contrary to these results, Banik et al. (2024) find that very wide binary stars disprove MOND. This was rebutted by Hernandez & Chae (2023), who stress that

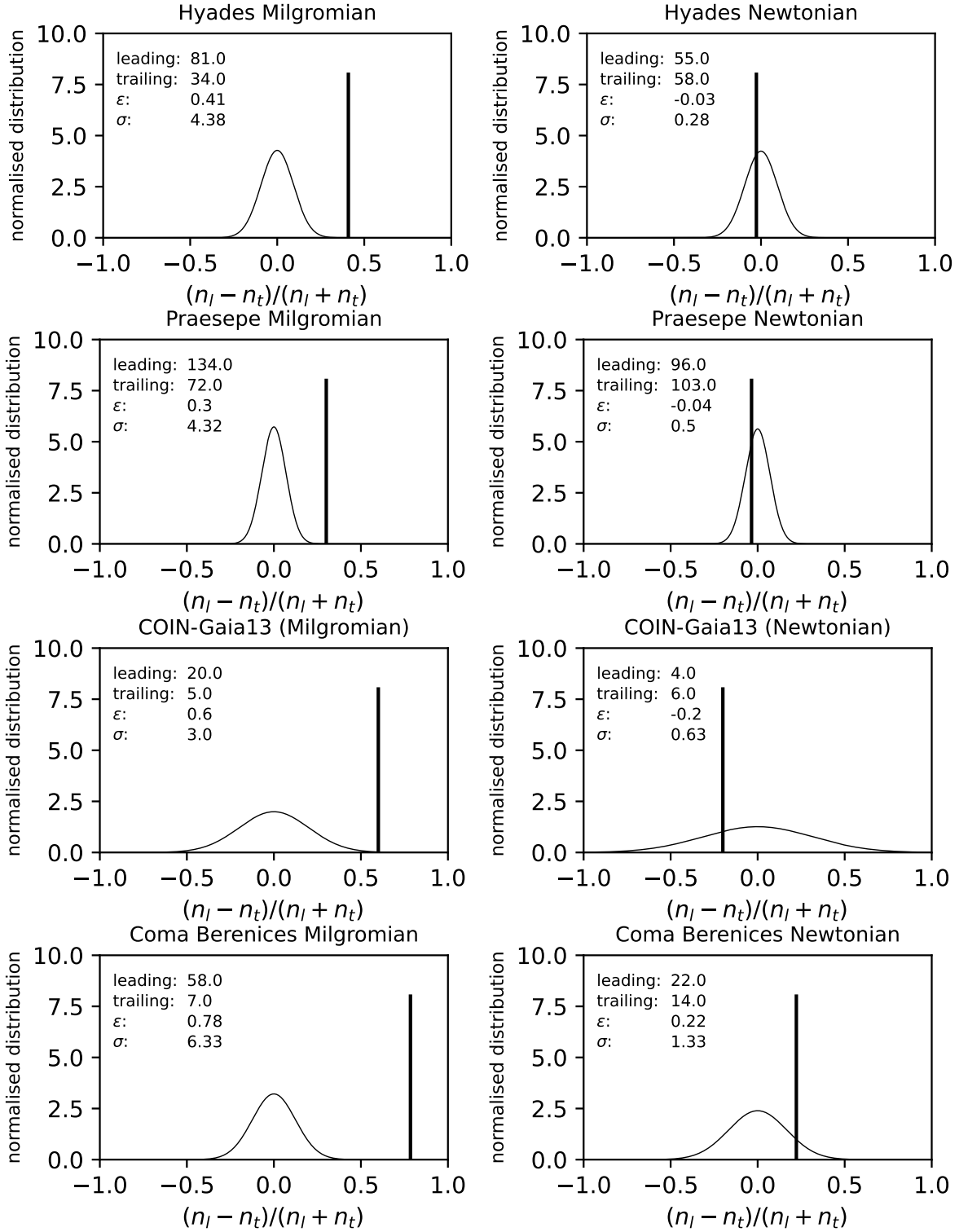


Figure 13. As Fig. 4 but here for the models (left/right panels for Milgromian/Newtonian). The leading and trailing tail numbers of the three stacked models for each case are combined to assess the probability whether all measurements are one-sided asymmetric with $n_l > n_t$. All Milgromian models are significantly asymmetric ($\sigma \geq 3.0$) with the leading tail containing more stellar particles than the trailing tidal tail and all Newtonian models are consistent with symmetrical tidal tails ($\sigma < 1.4$). These Newtonian values are consistent with those obtained in Sec. 4.1 using the PeTaR N -body code.

the sub-sample of close wide-binaries need to be shown by the same method to comply with Newtonian solu-

tions. This gauging of the wide-binary-star test was not demonstrated by Banik et al. (2024). While the align-

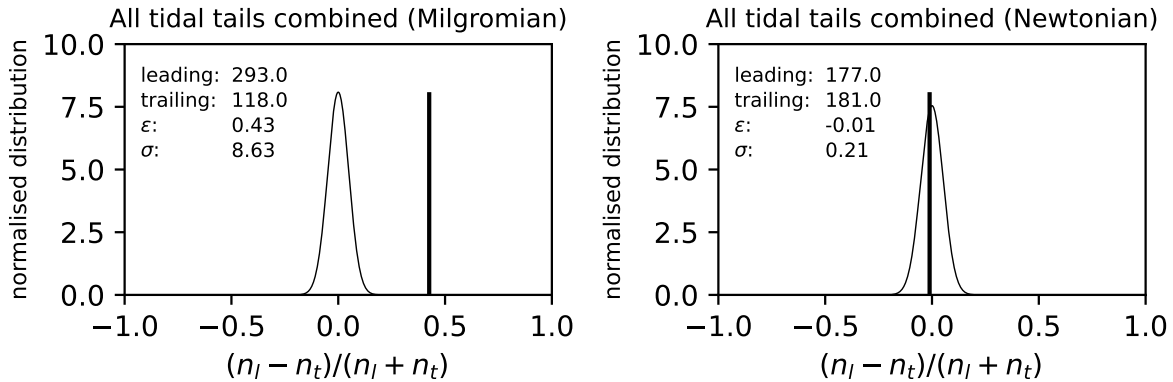


Figure 14. Similar to Fig. 13. Here the leading and trailing tail numbers of all models are combined to assess the probability if all measurements are one-sided asymmetric with $n_l > n_t$. The left panel depicts the combined stacked Milgromian models and shows a similar and extremely significant asymmetry that is very comparable to that observed (Fig. 9), while the combined stacked Newtonian models (right panel) are consistent with the leading and trailing tail having a similar number of stars.

ment of orbital elements of outer Solar System bodies are reported to probably be due to MOND (Paučo & Klačka 2016; Paučo 2017; Brown & Mathur 2023), Vokrouhlický et al. (2024) find this to not be possible, and on the Saturnian distance scale Desmond et al. (2024) report problems of matching the planet position data with Milgromian dynamics. Relevant in this work is that the field-equation underlying MOND (Sec. 4) needs a discretised analogy for the application to few-body dynamics which so-far has not been discovered. The technical details of the above modelling on the scale of thousands of AU may thus contain inconsistencies such that the conclusion reached on the validity or non-validity of Milgromian dynamics in this regime remain to be questionable (Pflamm-Altenburg 2024).

It would appear to be implausible that Milgromian dynamics be valid rather than Newtonian dynamics and that dark matter particles that are not part of the standard model of particle physics also exist. Indeed, apart from the above and apart from the fact that dark matter particles have not been found experimentally despite 40 yr of search, tests for the existence of dark matter particles that had been hoped to be accounting for the apparent non-Newtonian phenomena on galaxy scales have been yielding negative results: the presence of dark matter halos has been significantly questioned by the properties of dwarf galaxies in the Fornax galaxy cluster (Asencio et al. 2022). Applying the Chandrasekhar dynamical friction test to various galaxy systems (Kroupa 2015; Kroupa et al. 2023), and most recently on the Milky-Way/Large-/Small-Magellanic-Cloud triple system (Oehm & Kroupa 2024), shows no orbital solutions to be possible as the systems merge too quickly to be consistent with their observed configuration in phase-space. Solutions without dark matter particles but with Milgromian potentials are readily obtained

though. Noteworthy in this context is that earlier work had already shown that the observed rotation curves of disk galaxies cannot be reproduced if the theoretically-predicted dark matter halos are assumed (McGaugh 2005; McGaugh et al. 2007), and elliptical galaxies take too long to assemble in the dark-matter-based structure formation models to be consistent with their rapid early formation (Eappen et al. 2022). Independently of the above results concerning Milgromian dynamics, these tests thus suggest that dark matter particles do not exist.

In summary, the overall data situation thus indicates that the validity of the universal law of Newtonian gravitation is challenged, with Milgromian dynamics apparently accounting for the observed celestial dynamics. Successful structure-formation simulations in a Milgromian cosmological model have been published (particle-based: Katz et al. 2013, and hydrodynamical: Wittenburg et al. 2023). The Milgromian-interpretation of dynamics requires significant further attention and the implications of these findings for galactic astrophysics and cosmology are major if confirmed by further research. Hereby we need to keep in mind that different formulations of MOND exist due to insufficient knowledge which formulation is correct, and that additional differences in the detailed dynamical phenomena arise through different transition functions which are also not well understood, and that it remains possible that the formulation of MOND as is known today may be a simplification of a deeper matter–space-time coupling not fully understood at the present. This might be the case for example if MOND is related to the properties of the quantum vacuum (e.g. Milgrom 1999) that may change under different conditions.

We thank an anonymous referee for very helpful comments. Vikrant Jadhav acknowledges support through the Alexander von Humboldt Foundation in the form of an AvH Research Fellowship. Wenjie Wu acknowledges support through a studentship from the stellar populations and dynamics research (SPODYR) group at the University of Bonn. We thank the DAAD-Bonn-Prague exchange programme at the University of Bonn

for support. Much of this manuscript was written at the Department of Astrophysics, Astronomy and Mechanics at Aristotle University of Thessaloniki, and PK thanks Padelis Papadopoulos and other institute members there for their kind hospitality. This work relies on data obtained by the Gaia astrometric space mission. Stacy McGaugh's Triton Station was an important source of information on the problem concerning the Gaia-DR3-derived Keplerian fall-off of the Galaxy's rotation curve.

REFERENCES

- Aarseth, S. J. 1963, *MNRAS*, 126, 223,
doi: [10.1093/mnras/126.3.223](https://doi.org/10.1093/mnras/126.3.223)
- . 1999, *PASP*, 111, 1333, doi: [10.1086/316455](https://doi.org/10.1086/316455)
- . 2010, *Gravitational N-Body Simulations*
- Aarseth, S. J., Henon, M., & Wielen, R. 1974, *A&A*, 37, 183
- Asencio, E., Banik, I., & Kroupa, P. 2021, *MNRAS*, 500, 5249, doi: [10.1093/mnras/staa3441](https://doi.org/10.1093/mnras/staa3441)
- Asencio, E., Banik, I., Mieske, S., et al. 2022, *MNRAS*, 515, 2981, doi: [10.1093/mnras/stac1765](https://doi.org/10.1093/mnras/stac1765)
- Bai, L., Zhong, J., Chen, L., Li, J., & Hou, J. 2022, *Research in Astronomy and Astrophysics*, 22, 055022, doi: [10.1088/1674-4527/ac60d2](https://doi.org/10.1088/1674-4527/ac60d2)
- Banerjee, S., Belczynski, K., Fryer, C. L., et al. 2020, *A&A*, 639, A41, doi: [10.1051/0004-6361/201935332](https://doi.org/10.1051/0004-6361/201935332)
- Banik, I., Pittordis, C., Sutherland, W., et al. 2024, *MNRAS*, 527, 4573, doi: [10.1093/mnras/stad3393](https://doi.org/10.1093/mnras/stad3393)
- Banik, I., Thies, I., Famaey, B., et al. 2020, *ApJ*, 905, 135, doi: [10.3847/1538-4357/abc623](https://doi.org/10.3847/1538-4357/abc623)
- Banik, I., Thies, I., Truelove, R., et al. 2022, *MNRAS*, 513, 129, doi: [10.1093/mnras/stac722](https://doi.org/10.1093/mnras/stac722)
- Banik, I., & Zhao, H. 2022, *Symmetry*, 14, 1331, doi: [10.3390/sym14071331](https://doi.org/10.3390/sym14071331)
- Baumgardt, H., & Makino, J. 2003, *MNRAS*, 340, 227, doi: [10.1046/j.1365-8711.2003.06286.x](https://doi.org/10.1046/j.1365-8711.2003.06286.x)
- Bekenstein, J., & Milgrom, M. 1984, *ApJ*, 286, 7, doi: [10.1086/162570](https://doi.org/10.1086/162570)
- Bílek, M., Thies, I., Kroupa, P., & Famaey, B. 2018, *A&A*, 614, A59, doi: [10.1051/0004-6361/201731939](https://doi.org/10.1051/0004-6361/201731939)
- Binney, J., & Tremaine, S. 1987, *Galactic dynamics*
- Boffin, H. M. J., Jerabkova, T., Beccari, G., & Wang, L. 2022, *MNRAS*, 514, 3579, doi: [10.1093/mnras/stac1567](https://doi.org/10.1093/mnras/stac1567)
- Bovy, J. 2015, *ApJS*, 216, 29, doi: [10.1088/0067-0049/216/2/29](https://doi.org/10.1088/0067-0049/216/2/29)
- Brown, K., & Mathur, H. 2023, *AJ*, 166, 168, doi: [10.3847/1538-3881/acef1e](https://doi.org/10.3847/1538-3881/acef1e)
- Capuzzo Dolcetta, R., Di Matteo, P., & Miocchi, P. 2005, *AJ*, 129, 1906, doi: [10.1086/426006](https://doi.org/10.1086/426006)
- Casertano, S., & Hut, P. 1985, *ApJ*, 298, 80, doi: [10.1086/163589](https://doi.org/10.1086/163589)
- Chae, K.-H. 2023, *ApJ*, 952, 128, doi: [10.3847/1538-4357/ace101](https://doi.org/10.3847/1538-4357/ace101)
- . 2024, *ApJ*, 960, 114, doi: [10.3847/1538-4357/ad0ed5](https://doi.org/10.3847/1538-4357/ad0ed5)
- Chae, K.-H., Desmond, H., Lelli, F., McGaugh, S. S., & Schombert, J. M. 2021, *ApJ*, 921, 104, doi: [10.3847/1538-4357/ac1bba](https://doi.org/10.3847/1538-4357/ac1bba)
- Chae, K.-H., Lelli, F., Desmond, H., et al. 2020, *ApJ*, 904, 51, doi: [10.3847/1538-4357/abbb96](https://doi.org/10.3847/1538-4357/abbb96)
- Chae, K.-H., & Milgrom, M. 2022, *ApJ*, 928, 24, doi: [10.3847/1538-4357/ac5405](https://doi.org/10.3847/1538-4357/ac5405)
- Desmond, H., Hees, A., & Famaey, B. 2024, *MNRAS*, 530, 1781, doi: [10.1093/mnras/stae955](https://doi.org/10.1093/mnras/stae955)
- Dinnbier, F., Kroupa, P., & Anderson, R. I. 2022, *A&A*, 660, A61, doi: [10.1051/0004-6361/202142082](https://doi.org/10.1051/0004-6361/202142082)
- Eappen, R., & Kroupa, P. 2024, *MNRAS*, 528, 4264, doi: [10.1093/mnras/stae286](https://doi.org/10.1093/mnras/stae286)
- Eappen, R., Kroupa, P., Wittenburg, N., Haslbauer, M., & Famaey, B. 2022, *MNRAS*, 516, 1081, doi: [10.1093/mnras/stac2229](https://doi.org/10.1093/mnras/stac2229)
- Famaey, B., & McGaugh, S. S. 2012, *Living Reviews in Relativity*, 15, 10. <https://arxiv.org/abs/1112.3960>
- Fürnkranz, V., Meingast, S., & Alves, J. 2019, *A&A*, 624, L11, doi: [10.1051/0004-6361/201935293](https://doi.org/10.1051/0004-6361/201935293)
- Haghi, H., Bazkiaei, A. E., Zonoozi, A. H., & Kroupa, P. 2016, *MNRAS*, 458, 4172, doi: [10.1093/mnras/stw573](https://doi.org/10.1093/mnras/stw573)
- Haslbauer, M., Banik, I., & Kroupa, P. 2020, *MNRAS*, 499, 2845, doi: [10.1093/mnras/staa2348](https://doi.org/10.1093/mnras/staa2348)
- Heggie, D., & Hut, P. 2003, *The Gravitational Million-Body Problem: A Multidisciplinary Approach to Star Cluster Dynamics*
- Heggie, D. C., & Aarseth, S. J. 1992, *MNRAS*, 257, 513, doi: [10.1093/mnras/257.3.513](https://doi.org/10.1093/mnras/257.3.513)
- Hernandez, X. 2023, *MNRAS*, 525, 1401, doi: [10.1093/mnras/stad2306](https://doi.org/10.1093/mnras/stad2306)
- Hernandez, X., & Chae, K.-H. 2023, *arXiv e-prints*, arXiv:2312.03162, doi: [10.48550/arXiv.2312.03162](https://doi.org/10.48550/arXiv.2312.03162)

- Hernandez, X., Cookson, S., & Cortés, R. A. M. 2022, *MNRAS*, 509, 2304, doi: [10.1093/mnras/stab3038](https://doi.org/10.1093/mnras/stab3038)
- Hernandez, X., Cortés, R. A. M., Allen, C., & Scarpa, R. 2019, *International Journal of Modern Physics D*, 28, 1950101, doi: [10.1142/S0218271819501013](https://doi.org/10.1142/S0218271819501013)
- Hernandez, X., Jiménez, M. A., & Allen, C. 2012, *European Physical Journal C*, 72, 1884, doi: [10.1140/epjc/s10052-012-1884-6](https://doi.org/10.1140/epjc/s10052-012-1884-6)
- Hernandez, X., Verteletskyi, V., Nasser, L., & Aguayo-Ortiz, A. 2024, *MNRAS*, 528, 4720, doi: [10.1093/mnras/stad3446](https://doi.org/10.1093/mnras/stad3446)
- Hurley, J. R., Pols, O. R., & Tout, C. A. 2000, *MNRAS*, 315, 543, doi: [10.1046/j.1365-8711.2000.03426.x](https://doi.org/10.1046/j.1365-8711.2000.03426.x)
- Hurley, J. R., Tout, C. A., & Pols, O. R. 2002, *MNRAS*, 329, 897, doi: [10.1046/j.1365-8711.2002.05038.x](https://doi.org/10.1046/j.1365-8711.2002.05038.x)
- Hut, P., Makino, J., & McMillan, S. 1995, *ApJL*, 443, L93, doi: [10.1086/187844](https://doi.org/10.1086/187844)
- Jerabkova, T., Boffin, H. M. J., Beccari, G., et al. 2021, *A&A*, 647, A137, doi: [10.1051/0004-6361/202039949](https://doi.org/10.1051/0004-6361/202039949)
- Jiao, Y., Hammer, F., Wang, H., et al. 2023, *A&A*, 678, A208, doi: [10.1051/0004-6361/202347513](https://doi.org/10.1051/0004-6361/202347513)
- Just, A., Berczik, P., Petrov, M. I., & Ernst, A. 2009, *MNRAS*, 392, 969, doi: [10.1111/j.1365-2966.2008.14099.x](https://doi.org/10.1111/j.1365-2966.2008.14099.x)
- Katz, H., McGaugh, S., Teuben, P., & Angus, G. W. 2013, *ApJ*, 772, 10, doi: [10.1088/0004-637X/772/1/10](https://doi.org/10.1088/0004-637X/772/1/10)
- Kokubo, E., Yoshinaga, K., & Makino, J. 1998, *MNRAS*, 297, 1067, doi: [10.1046/j.1365-8711.1998.01581.x](https://doi.org/10.1046/j.1365-8711.1998.01581.x)
- Kraljic, D., & Sarkar, S. 2015, *JCAP*, 2015, 050, doi: [10.1088/1475-7516/2015/04/050](https://doi.org/10.1088/1475-7516/2015/04/050)
- Kroupa, P. 1997, *NewA*, 2, 139, doi: [10.1016/S1384-1076\(97\)00012-2](https://doi.org/10.1016/S1384-1076(97)00012-2)
- . 2001, *MNRAS*, 322, 231, doi: [10.1046/j.1365-8711.2001.04022.x](https://doi.org/10.1046/j.1365-8711.2001.04022.x)
- . 2008, *Initial Conditions for Star Clusters*, ed. S. J. Aarseth, C. A. Tout, & R. A. Mardling, Vol. 760, 181, doi: [10.1007/978-1-4020-8431-7_8](https://doi.org/10.1007/978-1-4020-8431-7_8)
- . 2015, *Canadian Journal of Physics*, 93, 169, doi: [10.1139/cjp-2014-0179](https://doi.org/10.1139/cjp-2014-0179)
- Kroupa, P., Aarseth, S., & Hurley, J. 2001, *MNRAS*, 321, 699, doi: [10.1046/j.1365-8711.2001.04050.x](https://doi.org/10.1046/j.1365-8711.2001.04050.x)
- Kroupa, P., Jerabkova, T., Thies, I., et al. 2022, *MNRAS*, 517, 3613, doi: [10.1093/mnras/stac2563](https://doi.org/10.1093/mnras/stac2563)
- Kroupa, P., Gjergo, E., Asencio, E., et al. 2023, *arXiv e-prints*, arXiv:2309.11552, doi: [10.48550/arXiv.2309.11552](https://doi.org/10.48550/arXiv.2309.11552)
- Küpper, A. H. W., Kroupa, P., Baumgardt, H., & Heggie, D. C. 2010, *MNRAS*, 401, 105, doi: [10.1111/j.1365-2966.2009.15690.x](https://doi.org/10.1111/j.1365-2966.2009.15690.x)
- Küpper, A. H. W., MacLeod, A., & Heggie, D. C. 2008, *MNRAS*, 387, 1248, doi: [10.1111/j.1365-2966.2008.13323.x](https://doi.org/10.1111/j.1365-2966.2008.13323.x)
- López-Corredoira, M., Betancort-Rijo, J. E., Scarpa, R., & Chrobáková, Ž. 2022, *MNRAS*, 517, 5734, doi: [10.1093/mnras/stac3117](https://doi.org/10.1093/mnras/stac3117)
- Makino, J. 1991, *ApJ*, 369, 200, doi: [10.1086/169751](https://doi.org/10.1086/169751)
- Mazurenko, S., Banik, I., Kroupa, P., & Haslbauer, M. 2024, *MNRAS*, 527, 4388, doi: [10.1093/mnras/stad3357](https://doi.org/10.1093/mnras/stad3357)
- McGaugh, S. S. 2005, *Physical Review Letters*, 95, 171302, doi: [10.1103/PhysRevLett.95.171302](https://doi.org/10.1103/PhysRevLett.95.171302)
- McGaugh, S. S., de Blok, W. J. G., Schombert, J. M., Kuzio de Naray, R., & Kim, J. H. 2007, *ApJ*, 659, 149, doi: [10.1086/511807](https://doi.org/10.1086/511807)
- McGaugh, S. S., & Wolf, J. 2010, *ApJ*, 722, 248, doi: [10.1088/0004-637X/722/1/248](https://doi.org/10.1088/0004-637X/722/1/248)
- Meingast, S., & Alves, J. 2019, *A&A*, 621, L3, doi: [10.1051/0004-6361/201834622](https://doi.org/10.1051/0004-6361/201834622)
- Merritt, D. 2020, *A Philosophical Approach to MOND: Assessing the Milgromian Research Program in Cosmology*
- Milgrom, M. 1983, *ApJ*, 270, 365, doi: [10.1086/161130](https://doi.org/10.1086/161130)
- . 1999, *Physics Letters A*, 253, 273, doi: [10.1016/S0375-9601\(99\)00077-8](https://doi.org/10.1016/S0375-9601(99)00077-8)
- . 2009, *ApJ*, 698, 1630, doi: [10.1088/0004-637X/698/2/1630](https://doi.org/10.1088/0004-637X/698/2/1630)
- . 2010, *MNRAS*, 403, 886, doi: [10.1111/j.1365-2966.2009.16184.x](https://doi.org/10.1111/j.1365-2966.2009.16184.x)
- Milgrom, M. 2014, *Scholarpedia*, 9, 31410, doi: [10.4249/scholarpedia.31410](https://doi.org/10.4249/scholarpedia.31410)
- Montuori, M., Capuzzo-Dolcetta, R., Di Matteo, P., Lepinette, A., & Miocchi, P. 2007, *ApJ*, 659, 1212, doi: [10.1086/512114](https://doi.org/10.1086/512114)
- Montuori, M., Capuzzo-Dolcetta, R., Matteo, P. D., & Miocchi, P. 2008, in *Astronomical Society of the Pacific Conference Series*, Vol. 390, *Pathways Through an Eclectic Universe*, ed. J. H. Knapen, T. J. Mahoney, & A. Vazdekis, 394, doi: [10.48550/arXiv.0709.0460](https://doi.org/10.48550/arXiv.0709.0460)
- Nagesh, S. T., Kroupa, P., Banik, I., et al. 2023, *MNRAS*, 519, 5128, doi: [10.1093/mnras/stac3645](https://doi.org/10.1093/mnras/stac3645)
- Oehm, W., & Kroupa, P. 2024, *Universe*, 10, doi: [10.3390/universe10030143](https://doi.org/10.3390/universe10030143)
- Ou, X., Eilers, A.-C., Necib, L., & Frebel, A. 2024, *MNRAS*, 528, 693, doi: [10.1093/mnras/stae034](https://doi.org/10.1093/mnras/stae034)
- Paučo, R. 2017, *A&A*, 603, A11, doi: [10.1051/0004-6361/201630335](https://doi.org/10.1051/0004-6361/201630335)
- Paučo, R., & Klačka, J. 2016, *A&A*, 589, A63, doi: [10.1051/0004-6361/201527713](https://doi.org/10.1051/0004-6361/201527713)
- Pflamm-Altenburg, J. 2024, submitted

- Pflamm-Altenburg, J., Kroupa, P., Thies, I., et al. 2023, *A&A*, 671, A88, doi: [10.1051/0004-6361/202244243](https://doi.org/10.1051/0004-6361/202244243)
- Pinfield, D. J., Jameson, R. F., & Hodgkin, S. T. 1998, *MNRAS*, 299, 955, doi: [10.1046/j.1365-8711.1998.01754.x](https://doi.org/10.1046/j.1365-8711.1998.01754.x)
- Piskunov, A. E., Kharchenko, N. V., Röser, S., Schilbach, E., & Scholz, R. D. 2006, *A&A*, 445, 545, doi: [10.1051/0004-6361:20053764](https://doi.org/10.1051/0004-6361:20053764)
- Plummer, H. C. 1911, *MNRAS*, 71, 460
- Röser, S., & Schilbach, E. 2019, *A&A*, 627, A4, doi: [10.1051/0004-6361/201935502](https://doi.org/10.1051/0004-6361/201935502)
- Röser, S., Schilbach, E., & Goldman, B. 2019, *A&A*, 621, L2, doi: [10.1051/0004-6361/201834608](https://doi.org/10.1051/0004-6361/201834608)
- Röser, S., Schilbach, E., Piskunov, A. E., Kharchenko, N. V., & Scholz, R. D. 2011, *A&A*, 531, A92, doi: [10.1051/0004-6361/201116948](https://doi.org/10.1051/0004-6361/201116948)
- Rossi, L. J., & Hurley, J. R. 2015, *MNRAS*, 454, 1453, doi: [10.1093/mnras/stv2039](https://doi.org/10.1093/mnras/stv2039)
- Safarzadeh, M., & Loeb, A. 2021, *ApJL*, 914, L37, doi: [10.3847/2041-8213/ac07aa](https://doi.org/10.3847/2041-8213/ac07aa)
- Sylos Labini, F., Chrobáková, Ž., Capuzzo-Dolcetta, R., & López-Corredoira, M. 2023, *ApJ*, 945, 3, doi: [10.3847/1538-4357/acb92c](https://doi.org/10.3847/1538-4357/acb92c)
- Tang, S.-Y., Pang, X., Yuan, Z., et al. 2019, *ApJ*, 877, 12, doi: [10.3847/1538-4357/ab13b0](https://doi.org/10.3847/1538-4357/ab13b0)
- Thomas, G. F., Famaey, B., Monari, G., et al. 2023, *A&A*, 678, A180, doi: [10.1051/0004-6361/202346650](https://doi.org/10.1051/0004-6361/202346650)
- Vokrouhlický, D., Nesvorný, D., & Tremaine, S. 2024, arXiv e-prints, arXiv:2403.09555, doi: [10.48550/arXiv.2403.09555](https://doi.org/10.48550/arXiv.2403.09555)
- Wang, H.-F., Chrobáková, Ž., López-Corredoira, M., & Sylos Labini, F. 2023, *ApJ*, 942, 12, doi: [10.3847/1538-4357/aca27c](https://doi.org/10.3847/1538-4357/aca27c)
- Wang, L., Iwasawa, M., Nitadori, K., & Makino, J. 2020, *MNRAS*, 497, 536, doi: [10.1093/mnras/staa1915](https://doi.org/10.1093/mnras/staa1915)
- Wittenburg, N., Kroupa, P., Banik, I., Candlish, G., & Samaras, N. 2023, *MNRAS*, 523, 453, doi: [10.1093/mnras/stad1371](https://doi.org/10.1093/mnras/stad1371)
- Wittenburg, N., Kroupa, P., & Famaey, B. 2020, *ApJ*, 890, 173, doi: [10.3847/1538-4357/ab6d73](https://doi.org/10.3847/1538-4357/ab6d73)